
CO₂ fluxes in the Northeast Atlantic Ocean based on measurements from a surface ocean observation platform

Curbelo-Hernández D ¹, González-Dávila M ^{1,*}, Gonzalez Ag ¹, González-Santana D ^{1,2},
Santana-Casiano Jm ¹

¹ Instituto de Oceanografía y Cambio Global, IOAG, Universidad de Las Palmas de Gran Canaria, 35017, Spain

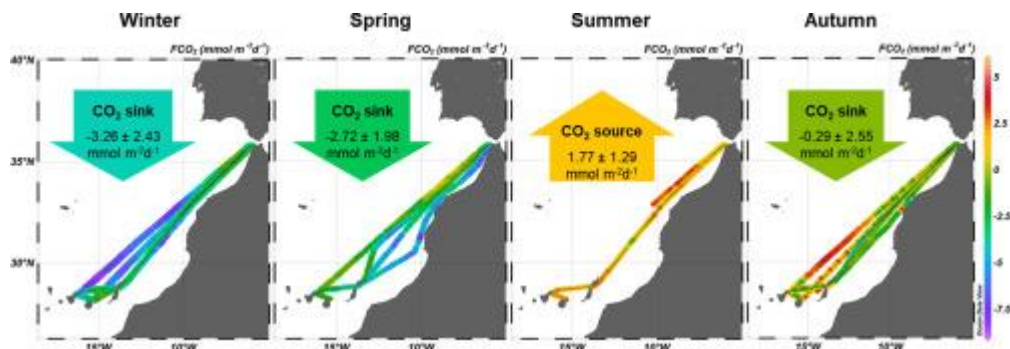
² Univ Brest, CNRS IRD, IFREMER, LEMAR, F-29280 Plouzane, France

* Corresponding author : M. González-Dávila, email address : melchor.gonzalez@ulpgc.es

Abstract :

The seasonal and spatial variability of the CO₂ system parameters and CO₂ air-sea exchange were studied in the Northeast Atlantic Ocean between the northwest African coastal upwelling and the oligotrophic open-ocean waters of the North Atlantic subtropical gyre. Data was collected aboard a volunteer observing ship from February 2019 to February 2020. The seasonal and spatial variability of CO₂ fugacity in seawater (fCO_{2,sw}) was strongly driven by the seasonal temperature variation, which increased with latitude and was lower throughout the year in coastal regions where the upwelling and offshore transport was more intense. The thermal to biological effect ratio (T/B) was approximately 2, with minimum values along the African coastline related to higher biological activity in the upwelled waters. The fCO_{2,sw} increased from winter to summer by $11.84 \pm 0.28 \mu\text{atm}^\circ\text{C}^{-1}$ on the inter-island routes and by $11.71 \pm 0.25 \mu\text{atm}^\circ\text{C}^{-1}$ along the northwest African continental shelf. The seasonality of total inorganic carbon normalized to constant salinity of 36.7 (NCT) was studied throughout the region. The effect of biological processes and calcification/dissolution on NCT between February and October represented >90% of the reduction of inorganic carbon while air-sea exchange described <6%. The seasonality of air-sea CO₂ exchange was controlled by temperature. The surface waters of the entire region acted as a CO₂ sink during the cold months and as a CO₂ source during the warm months. The Canary basin acted as a net sink of $-0.26 \pm 0.04 \text{ molC m}^{-2} \text{ yr}^{-1}$. The northwest African continental shelf behaved as a stronger sink at $-0.48 \pm 0.09 \text{ molC m}^{-2} \text{ yr}^{-1}$. The calculated average CO₂ flux for the entire area was $-2.65 \pm 0.44 \text{ TgCO}_2 \text{ yr}^{-1}$ ($-0.72 \pm 0.12 \text{ TgC yr}^{-1}$).

Graphical abstract



Highlights

► The SST controls the seasonal and spatial variation of CO₂ fugacity and fluxes. ► The pH and *f*CO₂ shows spatial variability associated with upwelling influence. ► NC_T variation was mainly governed by biological activity and slightly affected by air-sea fluxes. ► During 2019, the Northeast Atlantic region behaved as an annual CO₂ sink of -2.65 ± 0.44 Tg CO₂ yr⁻¹. ► VOS lines are a powerful tool to study de CO₂ system and fluxes in the coastal surface area.

Keywords : CO₂ system, air-sea CO₂ exchange, Northeast Atlantic, northwest African coastal upwelling, surface ocean observation platform.

1. Introduction

The Earth's oceans are an important carbon sink, removing about one third of the total CO₂ emissions from the atmosphere (Friedlingstein et al., 2019; Gruber et al., 2019; Le Quéré et al., 2018). A decrease in pH and an alteration of the fundamental chemical balances have been observed in the global ocean as a consequence of this CO₂ uptake (Bates et al., 2014; Doney et al., 2009), affecting marine ecosystems and living organisms (Gattuso and Hansson, 2011). In this context, coastal regions and continental shelves, which are biogeochemically active regions, play an important role in the global carbon cycle. They are characterised by carbon fixation and remineralisation rates higher than the global average and by high spatial and temporal variability of the CO₂ fluxes (Borges et al., 2005; Cai et al., 2006; Frankignoulle and Borges, 2001; Shedwick et al., 2010; 2011). These regions have been largely ignored in the Global Carbon Budget due to the limited number of local and regional studies and the resulting poor representation in global models. Borges et al. (2005) highlighted the importance of coastal areas in the Global Carbon Budget. They remarked that the inclusion of coastal zones increased the estimated global ocean CO₂ sinks by 57% at high latitudes and by 15% in mid-latitudes, while CO₂ emissions from the ocean to the atmosphere increased by 13% in tropical and subtropical regions. This is a consequence of the latitudinal variability of air-sea CO₂ exchange on the continental shelves: medium- and high-latitude continental shelves acts as net sinks (-0.33 Pg C yr⁻¹) and low-latitude shelves act as net sources (0.11 Pg C yr⁻¹) (Borges et al., 2005; Cai et al., 2006; Chen et al., 2013). The net carbon flux on the continental shelves ranges between ~0.25 Pg C yr⁻¹ (Cai, 2011) and 0.4 Pg

C yr⁻¹ (Chen et al., 2013). However, these results were obtained from scalar approximations and interpolations and show a high degree of uncertainty due to the limited available data. A higher number of regional carbon cycle studies with a high measurement frequency are required in coastal areas and continental shelves in order to improve the characterization of the Global Carbon Budget.

The North Atlantic has been recognized as one of the largest ocean sinks of natural and anthropogenic CO₂, especially at subtropical and subpolar latitudes (e.g. Jing et al., 2019; Khatiwala et al., 2013; Leseurre et al., 2020; Sabine et al., 2004; Takahashi et al., 2002; Takahashi et al., 2009). This basin stores 23% of the global oceanic anthropogenic CO₂ despite covering only 15% of the global ocean area due to high vertical integration driven by deep water mass formation processes and thermohaline circulation (THC) (Sabine et al., 2004). The greatest source of uncertainty in the North Atlantic Carbon Budget is the contribution of the seasonal and spatial variability of CO₂ system and air-sea exchange in coastal waters and on continental shelves, especially in the Eastern Boundary Upwelling Systems.

The seasonal variability of CO₂ on the European continental shelf was studied by using a high temporal resolution (Frankignoulle and Borges, 2001). The European continental shelf acts as a net sink ranging from -0.09 to -0.17 Pg C yr⁻¹. A similar characterization on the African continental shelf in the North Atlantic is difficult to perform due to the low temporal resolution of the available regional studies. Studies in the Northeast Atlantic are essential to understand the biogeochemical dynamics in the coastal transition region of the northwest African upwelling, with high rates of primary production and carbon recycling and export (Huntsman and Barber, 1977; Jewell, 1994). The strong influence on the intensity and location of the Canary Current (Pelegri et al., 2005), the effect of the CO₂ continental pump (Tsunogai et al., 1999) and the oligotrophic ocean waters of the North Atlantic subtropical

gyre should also be considered. Offshore export of the upwelling physicochemical characteristics through superficial cold-water filaments can reach several hundred kilometres during the warm months, coinciding with the maximum intensity of the upwelling between the Canary Islands and the Strait of Gibraltar (Pelegrí et al., 2005). The seasonal variations of the CO₂ parameters in the Northeast Atlantic subtropical gyre have been studied at the European Station of Oceanic Time Series (ESTOC) (González-Dávila et al., 2003; González-Dávila et al., 2010; Santana-Casiano et al., 2007). The results show the effects of seasonality, mainly due to temperature dependence of the CO₂ system parameters at the ESTOC site, acting as a CO₂ sink during the cold months (December-May) and as a source during the warm months (June-November) (González-Dávila et al., 2003; Santana-Casiano et al., 2001). The aim of this study was to analyse the behaviour and distribution of CO₂ in the Northeast Atlantic region between the Canary Islands and the Strait of Gibraltar from February 2019 to February 2020. The first objective was to obtain high frequency measurements and data through autonomous monitoring systems deployed on a surface ocean observing platform (SOOP) on a volunteer observing ship (VOS), SOOP CanOA-VOS. Samples were analysed on the Canary basin and on the African continental shelf (Fig. 1) and discussed considering surface data collected by other VOS and research vessels in the Northeast Atlantic (26-38°N, 5-20°W) (SOCAT v2020).

2. Material and methods

Seasonal variability in the distribution and air-sea exchange of CO₂ was studied in the oceanic waters of the Canary archipelago and in the transitional waters between the northwest African coastal upwelling and the oceanic waters of the North Atlantic subtropical gyre. The high spatial and temporal data was obtained using automated underway systems aboard the SOOP CanOA container ship RENATE P (IMO: 9144718), a VOS operated by Nisa Maritime. The vessel has a usual route which stops at three ports in the Canary Islands (Las

Palmas de Gran Canaria (28.1319°N, 15.4185°W; GC), Santa Cruz de Tenerife (28.4867°N, 16.2284°W; TNF), Arrecife (28.9682°N, 13.5294°W; LNZ), and travel northward towards the Mediterranean Sea crossing the Strait of Gibraltar (SG). The data was collected with a frequency of two weeks (time required to perform a round trip) at the port of Las Palmas de Gran Canaria. This study focused on the Northeast Atlantic Ocean and was divided into two regions. First, the oceanographic environment of the Canary Islands, between Gran Canaria and Tenerife (GC-TNF) and between Tenerife and Lanzarote (TNF-LNZ). Second, the coastal region and transition to ocean waters of northwest Africa between the Canary Islands and the Strait of Gibraltar (CI-SG).

2.1. Temperature, salinity and xCO₂ measurements

An automated underway seawater and low atmospheric CO₂ molar fraction (xCO₂) measurement system, developed by Craig Neill and commercialized by General Oceanics™, with additional sensors of temperature, salinity and oxygen, was installed inside the engine room of the RENATE P container ship. The system combines an air and water equilibrator with an infrared analyser for detection, which produces comparable and high quality data sets (Pierrot et al., 2009).

The system calibration was carried out automatically on departure from and arrival at each port, and periodically every three hours during the ship's journey, with four standard gases (0 ppm, 249.37 ppm, 397.83 ppm and 524.74 ppm) provided by the National Ocean and Atmospheric Administration (NOAA) and traceable to the World Meteorological Organization (WMO).

Measurements of xCO₂ (ppm) in seawater with frequencies of 2-3 minutes were performed by extracting seawater from the ship's supply at flow rates greater than 60 L min⁻¹ and passing it through a plexiglass equilibrator at flow rates ranging between 3 and 4 L min⁻¹. The system also performs three xCO₂ measurements in low atmosphere per hour used to compute

atmospheric CO₂ content. In both cases, a non-dispersive infrared analyser built by LICOR[®] (initially the 6262 model and after October 2019, a 7000 model) were used for the detection of xCO₂.

The sea surface temperature (SST, in °C) was measured using a SBE38 thermometer placed at the main seawater intake not affected by the ship engine. A SBE21 thermosalinograph (TSG), with an estimated error of 0.01°C, was located near the xCO₂ system. In addition, the temperature in the equilibrator was monitored due to the high sensitivity of xCO₂ to temperature changes. Sea surface salinity (SSS) was measured with a manually calibrated SBE21 thermosalinograph, with an estimated error of ±0.005. Atmospheric pressure was measured by the deck's transducer (these pressure records being different in the order of millibars with the pressure near the xCO₂ system, inside the ship).

Due to technical problems with the measurement equipment aboard the VOS, no temperature, salinity or xCO₂ measurements were obtained during March 2019 (problems with water intake), during the second half of August 2019 (problems with LICOR flow) and on a limited number of return journeys from the port of Barcelona.

2.2. Variable determination

This study followed the data collection methodology, quality control and calculation procedures as published in the updated version of the DOE method manual for carbon dioxide analysis in seawater (Dickson et al., 2007). From the measured and corrected values, the fugacity of CO₂ was calculated in seawater ($f\text{CO}_{2,\text{sw}}$) and the lower atmosphere ($f\text{CO}_{2,\text{atm}}$) following the procedure as indicated by Pierrot et al. (2009).

The partial effect of thermal and non-thermal factors on seasonal variation of $f\text{CO}_{2,\text{sw}}$ was studied using the equations presented by Takahashi et al. (2002), with the temperature effects on $f\text{CO}_{2,\text{sw}}$ for isochemical seawater of $0.0423^\circ\text{C}^{-1}$ determined experimentally by Takahashi et al. (1993) for a North Atlantic surface water sample. To study the non-thermal effect, termed

in this work as biological effect, $f\text{CO}_{2,\text{sw}}$ was normalized to the average temperature (Eq. 1) to remove the temperature effect. The biological effect was obtained from the seasonal amplitude of the normalized $f\text{CO}_{2,\text{sw}}$ (Eq. 2). The thermal effect was calculated by computing the average value of $f\text{CO}_{2,\text{sw}}$ to the observed temperature (Eq. 3) and determining its seasonal amplitude (Eq. 4). The relative importance of thermal and biological effects was expressed by the T/B ratio $[(\Delta f\text{CO}_2)_{\text{temp}}/(\Delta f\text{CO}_2)_{\text{bio}}]$, where values greater than 1 indicated that the temperature effect dominated over the biological effect.

$$f\text{CO}_2 (T_{\text{mean}}) = (f\text{CO}_2)_{\text{obs}} \cdot \exp[0.0423(T_{\text{mean}} - T_{\text{obs}})] \quad (1)$$

$$(\Delta f\text{CO}_2)_{\text{bio}} = [f\text{CO}_2 (T_{\text{mean}})]_{\text{max}} - [f\text{CO}_2 (T_{\text{mean}})]_{\text{min}} \quad (2)$$

$$f\text{CO}_2 (T_{\text{obs}}) = (f\text{CO}_2)_{\text{mean}} \cdot \exp[0.0423(T_{\text{obs}} - T_{\text{mean}})] \quad (3) (\Delta f\text{CO}_2)_{\text{temp}} =$$

$$[f\text{CO}_2 (T_{\text{obs}})]_{\text{max}} - [f\text{CO}_2 (T_{\text{obs}})]_{\text{min}} \quad (4)$$

The CO_2 fluxes (FCO_2) were determined using Eq. 5:

$$\text{FCO}_2 = 0.24 \cdot S \cdot k \cdot \Delta f\text{CO}_2 \quad (5)$$

where 0.24 is a conversion factor to express data in $\text{mmol m}^{-2}\text{d}^{-1}$; S is the solubility of CO_2 in seawater and $\Delta f\text{CO}_2$ is the difference between the seawater and low atmosphere $f\text{CO}_2$ ($f\text{CO}_{2,\text{sw}} - f\text{CO}_{2,\text{atm}}$). Negative fluxes indicate that the ocean acts as an atmospheric CO_2 sink, while the positive ones indicate that it behaves as a source. The parameterization of Wanninkhof (2014) was used in this study, with k being the gas transfer rate expressed in Eq. 6:

$$k = 0.251 \cdot w^2 \cdot \left(\frac{Sc}{660}\right)^{-0.5} \quad (6)$$

where w is the wind speed (m s^{-1}) and Sc is Schmidt number (cinematic viscosity of seawater, divided by the gas diffusion coefficient).

For the FCO_2 calculations, daily averages of ocean surface wind speed were used with spatial resolution of $0.25^\circ \times 0.25^\circ$ derived from the Advanced Scatterometer (ASCAT) and obtained from the Satellite Research and Exploitation Center (CERSAT), at IFREMER, Plouzane

(France). These wind data were interpolated based on the latitude, longitude and date of the VOS line.

In addition, 54 surface water samples were manually taken along the route during February 2020 with a temporal frequency of 4 hours and in situ measurements of SST and SSS. Samples from the intake seawater line were taken in borosilicate glass bottles, overfilled, preserved with 100 μl of saturated HgCl_2 , kept in darkness and analysed just after arriving at port, in a period less than 2 weeks. The total alkalinity (A_T , $\mu\text{mol kg}^{-1}$) was determined following the methodology described by Mintrop et al. (2000) with an accuracy of $\pm 1.5 \mu\text{mol kg}^{-1}$. The A_T was also calculated according to the global relationships of A_T with SSS and SST in global surface waters described by Lee et al. (2005), for the subtropical ocean (30°S-30°N) and the North Atlantic (30°N-80°N) for the measurements taken on the inter-island routes and on the Canary Islands-Strait of Gibraltar route, respectively.

The A_T values obtained from the analysed samples and those calculated presented an average difference of $3.26 \pm 0.28 \mu\text{mol kg}^{-1}$. Due to the similarity of both values, A_T was calculated using the fitting equation of the A_T values obtained from discrete samples (Eq. 7) (temperature was not found to improve the fitting of the experimental data). It was assumed that the A_T -SSS relationship is valid throughout the full year in tropical and subtropical latitudes (Lee et al., 2005).

$$A_T = 1990.5003 + 456.6909 \cdot (\text{SSS} - 35) - 125.2005 \cdot (\text{SSS} - 35)^2 \quad (7)$$

From the A_T and $f\text{CO}_2$ values, the Total Dissolved Inorganic Carbon (C_T , $\mu\text{mol kg}^{-1}$) and pH in total scale (pH_T) were computationally determined with the Excel program CO_2sys , using the carbonic acid dissociation constants of Lueker et al. (2000), the HSO_4 dissociation constant of Dickson (1990) and the value of $[\text{B}]_1$ determined by Lee et al. (2010).

The temporal variation of C_T was studied using the equation of Sarmiento and Gruber, (2006) (Eq. 8). This equation describes the change in C_T over time produced by air-sea CO_2

exchange (EX), horizontal and vertical advection (TRSP), net community production (NCP), horizontal and vertical diffusion (DIFF) and vertical entrainment from the mixed layer (ENT).

$$\frac{dNC_T}{dt} = \frac{dNC_T}{dt} |_{EX} + \frac{dNC_T}{dt} |_{TRSP} + \frac{dNC_T}{dt} |_{NCP} + \frac{dNC_T}{dt} |_{DIFF} + \frac{dNC_T}{dt} |_{ENT} \quad (8)$$

The NC_T variation was studied between February and October, when C_T decreased and the vertical mixing with the underlying layers of the thermocline were suppressed due to the increase in stratification of the surface waters and the decrease in the mixed layer depth (MLD) (González-Dávila et al., 2003; Santana-Casiano et al., 2007). The observed C_T growth period between October and February was excluded due to lack of C_T values at the bottom of the MLD. The vertical diffusion at BATS (Gruber et al., 1998) and ESTOC (González-Dávila et al., 2003) was found to be small. Therefore, the vertical entrainment and diffusion terms were omitted. The change in NC_T was calculated as the difference between two consecutive months and was expressed in mmol m^{-3} , considering the seawater density. Negative values were indicative of a decrease of NC_T in surface waters. The air-sea CO_2 exchange (EX) term was obtained from the relationship between FCO_2 and MLD. The annual climatological monthly MLD was estimated from a variable temperature threshold of 0.2°C and obtained at IFREMER with a spatial resolution of $2 \times 2^\circ$ (Boyer Montégut et al. 2004, 2007, Mignot et al. 2007). The annual MLD cycle in the Northeast Atlantic was fitted to the harmonic Eq. 9 (latitude was not found to improve the fitting of the monthly MLD data).

$$MLD = 55.55 - 35.49 \cdot \cos(1.555 \cdot \text{days}) - 17.59 \cdot \sin(1.555 \cdot \text{days}) \quad (9)$$

The MLD variation range estimated for the ESTOC site (1995-2004) by Santana-Casiano et al. (2007) following Brainerd and Gregg, (1995) was used, with minimum and maximum depth values of 25 and 120 meters for the periods of September-October and February-March, respectively, and considering the harmonic decrease of MLD given by Eq. 9 between February and October, 2019. For the horizontal transport component (TRSP), the difference

between African coastal and oceanic stations selected in a similar latitude range ($\Delta NC_T = NC_{T, \text{(coastal waters)}} - NC_{T, \text{(oceanic waters)}}$) were considered. The NC_T was estimated at both stations taking into account the spatial change in salinity using the C_T -Salinity fit line at the most coastal point. The NC_T variation by horizontal advection was obtained from the product of ΔNC_T and the change in salinity with time at the most oceanic point. Positive values indicated that horizontal transport occurred from coastal upwelled waters to oceanic waters through surface filaments, while negative values indicated that the transport direction was reversed. Lastly, the change in NC_T due to biological processes (NC_P) considered the sum of changes in calcification/dissolution and photosynthesis/respiration processes and was obtained directly from Eq. 8. Negative values indicate a decrease in NC_T due to uptake (primary production) and calcification, while positive values reveal an increase in NC_T due to remineralization and dissolution.

2.3. Computational methods

The raw output data was initially filtered eliminating data stations affected by the automatic sampler such as samples measured at low water flow rates ($< 2.5 \text{ L min}^{-1}$). The measured xCO_2 values were corrected following the indication of Pierrot et al. (2009), linearly interpolating the standard values with the xCO_2 measurement times and performing a linear regression using a least squares analysis to obtain the corrected xCO_2 value in relation to the certified standard values (section 2.2.). The three $fCO_{2,atm}$ values obtained after each calibration were averaged and linearly interpolated with the times of each $fCO_{2,sw}$. The ΔfCO_2 was computed from the difference between the $fCO_{2,sw}$ and the $fCO_{2,atm}$ values and was used in the FCO_2 calculations (section 2.2).

The processed data were divided according to the three journeys of interest: GC-TNF, TNF-LNZ and CI-SG. To study the seasonal variability, SST, SSS, C_T , $fCO_{2,sw}$, FCO_2 and pH_T values were averaged every 0.05° of longitude on the GC-TNF route, 0.1° of longitude on the

TNF- LNZ route and 0.25° of latitude on the CI-SG route. The annual and seasonal average were estimated as a function of latitude or longitude, respectively.

The temporal distribution of the variables of interest was calculated using strategic stations on each route. The average physicochemical variables (y) for each location were fitted to harmonic functions (Eq. 10) as a function of time (x) in order to study the seasonal variability and the thermal and non-thermal effect in $f\text{CO}_{2,\text{sw}}$ (Lüger et al., 2004; Takahashi et al., 2002). Coefficients $a-e$ for all the physicochemical variables studied on each route are available in Table A.1.

$$y = a + b \cdot \cos(2\pi x) + c \cdot \sin(2\pi x) + d \cdot \cos(4\pi x) + e \cdot \sin(4\pi x) \quad (10)$$

The results were compared to surface data collected by other VOS and research vessels in the Northeast Atlantic (26-38°N, 5-20°W) and available at the Surface Ocean CO₂ Atlas (SOCAT v2020, <https://www.socat.info/>) for the North Atlantic, Tropical Atlantic and Coastal Regions. The available SOCAT data for the period 1991-2019 were used to study the monthly frequency and the annual cycle of $f\text{CO}_{2,\text{sw}}$ in 2019 by considering an interannual rate of increase of 1.8 μatm per elapsed year (Bates et al., 2014). SST satellite images were obtained from Marine Copernicus database (<https://marine.copernicus.eu/>).

3. Results

The determined ($f\text{CO}_2$) and computed (C_T , pH_T and FCO_2) variables allowed for the determination of the seasonal and spatial variability of the CO₂ system and fluxes in the Northeast Atlantic Ocean. We considered three routes: Gran Canaria-Tenerife (GC-TNF), Tenerife-Lanzarote (TNF-LNZ) and Canary Islands-Strait of Gibraltar (CI-SG). The seasonal variability of $f\text{CO}_{2,\text{sw}}$ due to the partial effect of temperature and biological activity at strategic stations on each of the routes received special attention in this study.

The annual and seasonal averages of the carbon variables (Table 1) show that the maximum SST values observed during late summer) on all routes coincided with maximum values of

$f\text{CO}_{2,\text{sw}}$ and FCO_2 and minimum values of pH_T . The seasonal average of C_T was also minimum at this time of the year (González-Dávila et al., 2003; Santana-Casiano et al., 2007). The average seasonal variation of SST and SSS along the African coast (3.95 ± 0.05 °C and 0.232 ± 0.004 , respectively) were higher than on the GC-TNF (3.16 ± 0.01 °C and 0.080 ± 0.012 , respectively) and the TNF-LNZ routes (3.23 ± 0.01 °C and 0.056 ± 0.004 , respectively). The highest values of SST and SSS throughout the year were found in the southernmost section of the study region. Moreover, the average seasonal variation of $f\text{CO}_{2,\text{sw}}$ and pH_T in the Canary waters (42.12 ± 0.07 μatm and 0.040 ± 0.001 units, respectively) turned out to be slightly lower than those obtained in the northwest African coastal waters (50.39 ± 1.13 μatm and 0.048 ± 0.001 units, respectively). Supplementary Figures A.1, A.2 and A.3 show the temporal and spatial distribution of the studied variables on each route. The C_T was normalized (NC_T) to a constant SSS of 36.7 (the annual average SSS for the entire region) to remove the effect of evaporation and precipitation. Similarly, the pH_T values were normalized to a constant temperature of 21.0 °C ($\text{pH}_{T,21}$) to remove the temperature dependence on the variation of pH_T (Santana-Casiano et al., 2001; González-Dávila et al., 2003). The $f\text{CO}_{2,\text{sw}}$ was normalized to the average SST of each route to study the thermal and non-thermal effect in their spatial and temporal distribution, as indicated in section 2.2.

3.1. Inter-island routes

From February 2019 to February 2020, 23 inter-island routes were completed between Gran Canaria and Tenerife (GC-TNF, 15.4°W-16.2°W), 17 between Tenerife and Lanzarote (TNF-LNZ, 16.2°W-13.5°W) and 2 between Gran Canaria and Lanzarote (GC-LNZ, 15.4°W-13.5°W); the latter were included with the TNF-LNZ route. The inter-island routes followed a latitudinal transect between 28.1°N and 29.0°N. The results showed temporal and longitudinal variation and were annually and seasonally averaged every 0.05° and 0.1° longitude on the GC-TNF and TNF-LNZ routes, respectively (Fig. 2).

The seasonal trends of CO₂ system parameters and fluxes both on the GC-TNF and the TNF-LNZ routes were similar and coincided with previous studies at ESTOC (González-Dávila et al., 2003; González-Dávila et al., 2010; Santana-Casiano et al., 2007). The maximum average seasonal variation (winter to summer values) of $f\text{CO}_{2,\text{sw}}$ and FCO_2 were $42.15 \pm 0.10 \mu\text{atm}$ and $5.56 \pm 0.01 \text{ mmol m}^{-2} \text{ d}^{-1}$, respectively, on the GC-TNF route and $42.09 \pm 0.02 \mu\text{atm}$ and $5.00 \pm 0.03 \text{ mmol m}^{-2} \text{ d}^{-1}$, respectively, on the TNF-LNZ route. The seasonality of pH_T was linked to changes in $f\text{CO}_{2,\text{sw}}$ and FCO_2 , with inverse seasonal trends of $f\text{CO}_{2,\text{sw}}$ and pH_T throughout the longitudinal transects. The maximum average variation of pH_T was 0.040 ± 0.001 units for both routes between winter and summer. However, once the temperature dependence was removed, the maximum average variation of $\text{pH}_{T,21}$ occurred between autumn and spring, decreasing by approximately 0.02 units (0.019 ± 0.001 and 0.024 ± 0.001 , respectively). The maximum variation range in Ca^{2+} was similar for both routes (13.14 ± 0.22 and $14.18 \pm 0.32 \mu\text{mol kg}^{-1}$) and took place between cold and warm months. Seasonal changes showed longitudinal differences on both the GC-TNF and the TNF-LNZ routes. The system behaved as a source of CO₂ in the warm months (June-November) and as a sink in the cold months (December-May), coinciding with maximum and minimum values of $f\text{CO}_{2,\text{sw}}$, respectively (Table 1).

3.1.1. Gran Canaria-Tenerife route (GC-TNF)

The seasonal variability of the variables along the GC-TNF route presented longitudinal differences between the westernmost area and the easternmost region, particularly in the warm months (Fig. 2). The seasonal averages of $f\text{CO}_{2,\text{sw}}$ and FCO_2 were higher in the westernmost section of the route (15.95-16.20°W) in autumn ($408.33 \pm 0.79 \mu\text{atm}$ and $1.16 \pm 0.15 \text{ mmol m}^{-2} \text{ d}^{-1}$), coinciding with the maximum registered temperatures ($22.22 \pm 0.03 \text{ }^\circ\text{C}$) (Fig. 2 and Fig. A.1). The maximum autumn average values of $f\text{CO}_{2,\text{sw}}$ and FCO_2 at 16.025°W were $410.45 \pm 0.72 \mu\text{atm}$ and $1.92 \pm 0.14 \text{ mmol m}^{-2} \text{ d}^{-1}$, respectively, decreasing

eastwardly to $399.52 \pm 0.60 \mu\text{atm}$ and $-0.85 \pm 0.13 \text{ mmol m}^{-2}\text{d}^{-1}$, respectively, at 15.925°W . This change in behaviour from source to sink within only 0.1° longitude can be explained by the location of this part of the route in a leeward area of the Anaga mountains, on the east coast of Tenerife.

In order to understand longitudinal differences, two stations were selected along the GC-TNF route: the first positioned in a coastal influenced area ($16.05 \pm 0.1^\circ\text{W}$) and the second in an open-ocean region ($15.7 \pm 0.1^\circ\text{W}$), in which FCO_2 was negative (sink) during most of the year except for the summer (Fig. 3). The highest SST and SSS values throughout the year and the greatest variability of FCO_2 occurred at the westernmost station. The SST, $f\text{CO}_{2,\text{sw}}$ and FCO_2 averages were calculated from September to October to observe autumn longitudinal differences. The westernmost station presented higher CO_2 variables ($23.05 \pm 0.06^\circ\text{C}$, $420.46 \pm 0.85 \mu\text{atm}$ and $3.55 \pm 0.13 \text{ mmol m}^{-2} \text{d}^{-1}$) than the easternmost station ($22.60 \pm 0.05^\circ\text{C}$, $416.89 \pm 0.59 \mu\text{atm}$ and $2.51 \pm 0.09 \text{ mmol m}^{-2} \text{d}^{-1}$). Values of pH_T and $\text{pH}_{\text{T},21}$ changed by 0.003 ± 0.001 and 0.004 ± 0.001 units, respectively, between the stations in the same period. An average spatial $f\text{CO}_{2,\text{sw}}$ difference of $1.60 \pm 0.27 \mu\text{atm}$ was obtained between westernmost and easternmost stations. The seasonal variation of $f\text{CO}_{2,\text{sw}}$ was driven by temperature, with the T/B ratio at the westernmost station being slightly higher than at the easternmost station (Table 2) due to the spatial difference in $\Delta f\text{CO}_{2,\text{temp}}$ (81.15 and $69.60 \mu\text{atm}$, respectively).

The C_T and NC_T presented a seasonal trend at both stations (Fig. 3), with the lowest annual average NC_T ($2102.97 \pm 1.30 \mu\text{mol kg}^{-1}$) located at the westernmost station with higher salinity values (36.788 ± 0.022). The trends show that the decrease in C_T and NC_T values took place on both inter-island routes between February-March and September-October, when MLD decreased and stratification increased due to surface warming (Santana-Casiano et al., 2007). As a result, vertical mixing of deep waters decreased. Between September and October, low SSS values (<36.5) were measured at $15.7 \pm 0.1^\circ\text{W}$, coinciding with slightly

lower values of SST and C_T (22.60 ± 0.05 °C and 2098.17 ± 1.88 $\mu\text{mol kg}^{-1}$, respectively) compared to the station $16.05 \pm 0.1^\circ\text{W}$ (23.05 ± 0.06 and 2100.86 ± 1.04 $\mu\text{mol kg}^{-1}$, respectively). This suggests that a cold and low salinity filament could be passing through this station during this period of the year and that the C_T would be depleted at the surface due to the increase in biological uptake.

3.1.2. Tenerife-Lanzarote (TNF-LNZ)

Longitudinal variations were observed on the TNF-LNZ route, especially during summer and autumn. The $f\text{CO}_{2,\text{sw}}$ and FCO_2 during summer were higher at approximately 16.0°W (426.77 ± 0.83 μatm and 2.51 ± 0.08 $\text{mmol m}^{-2} \text{d}^{-1}$), coinciding with the maximum SST (22.93 ± 0.05 °C) (Fig. 2 and Fig. A.2). The average decrease in $f\text{CO}_{2,\text{sw}}$ during summer between the westernmost and the easternmost section (16.05°W and 13.55°W) was ~ 6.02 μatm and led to an increase in pH_T and $\text{pH}_{T,21}$ of 0.006 ± 0.001 and 0.011 ± 0.001 units, respectively. The $f\text{CO}_{2,\text{sw}}$ and FCO_2 in the easternmost section of the route increased during autumn within the channel between Lanzarote and Fuerteventura and in coastal waters to the south of Lanzarote. During autumn, the surface waters changed from being a CO_2 sink to being a powerful CO_2 source similar to what was observed during summer in the same location, with an increase in FCO_2 from -0.64 ± 0.10 to 2.57 ± 0.15 $\text{mmol m}^{-2} \text{d}^{-1}$ between 14.15°W and 13.55°W . SST and SSS were relatively constant in the westernmost part of the route and decreased eastwardly during all seasons. The maximum variations of SST and SSS (-0.52 ± 0.02 °C and -0.11 ± 0.03 , respectively) with respect to the average (20.99 ± 0.05 °C and 36.75 ± 0.06 , respectively) were observed in the easternmost section around the channel between Lanzarote and Fuerteventura, in a region close to the African continental shelf and influenced by filament incursion. In the westernmost sector, protected by the eastern islands from filament incursions (Davenport et al., 1999), the maximum variations of SST and SSS were 0.5 ± 0.02 °C and 0.07 ± 0.04 , respectively.

Four stations along the TNF-LNZ route ($15.6 \pm 0.1^\circ\text{W}$, $15.0 \pm 0.1^\circ\text{W}$, $14.5 \pm 0.1^\circ\text{W}$ and $13.9 \pm 0.1^\circ\text{W}$) were selected (Fig. 4). The results obtained for the three westernmost stations with the lowest coastal influence were similar to those obtained on the GC-TNF route. At $13.9 \pm 0.1^\circ\text{W}$, in a shallower region within the Lanzarote and Fuerteventura channel, annual average of SST ($20.57 \pm 0.10^\circ\text{C}$) and SSS (36.652 ± 0.023) were lower ($0.33\text{-}0.53^\circ\text{C}$ and $0.109\text{-}0.140$) than at the other stations due to the decrease of the bottom depth and its greater exposure to cold and less salinity water filaments. The highest seasonal FCO_2 variability was observed at the easternmost station, with maximum outgassing from June to October ($2.53 \pm 0.15 \text{ mmol m}^{-2} \text{ d}^{-1}$). Seasonal variability of $f\text{CO}_{2,\text{sw}}$ was mainly driven by thermal effects at all the stations. The T/B ratios (Table 2) show that temperature control dominated over biological activity at the westernmost stations. The seasonal variability of pH_T was driven by the change in $f\text{CO}_{2,\text{sw}}$ and was also greater at the westernmost and easternmost point. When the temperature dependence on pH_T was removed, the maximum variability of $\text{pH}_{T,21}$ was observed at stations $15.0 \pm 0.1^\circ\text{W}$ and $14.5 \pm 0.1^\circ\text{W}$. Values of $\text{pH}_{T,21}$ were higher at $15.6 \pm 0.1^\circ\text{W}$ during the cold months, while minimum values were registered at $13.9 \pm 0.1^\circ\text{W}$ throughout the year.

The C_T variation (Fig. 4) was similar at all stations and coincided with that observed on the GC-TNF route (Fig. 3). The NC_T change ranged between ~ 2090 and $\sim 2015 \mu\text{mol kg}^{-1}$ at all stations except for the stations located within the channel between Lanzarote and Fuerteventura, where NC_T ranged between ~ 2105 and $\sim 2120 \mu\text{mol kg}^{-1}$, due to a higher mixing with deep rich CO_2 water.

3.2. Canary Islands-Strait of Gibraltar route (CI-SG)

27 transects were completed between the Canary Islands and the entry of the Strait of Gibraltar ($\sim 28.1\text{-}35.8^\circ\text{N}$). These transects were used to study the seasonal and spatial variability of the CO_2 system and air-sea exchange in transitional waters between the

northwest African coastal upwelling and the oligotrophic open-ocean waters of the North Atlantic subtropical gyre. The usual route of the vessel runs at an approximate distance of 2-4° of longitude from the African coastline at its furthest point around the Bay of Agadir and Cape Ghir latitude (~30.6°N) and between 0.5 and 1.5° of longitude at its closest point around the Cape Beddouza latitude (~32.5°N). Only during April 2019, the vessel was close to the African coastline (~0.5° of longitude) along the area of maximum upwelling between Cape Ghir and Beddouza.

The temporal and latitudinal distribution of the results (Fig. A.3) shows a seasonality similar to that observed in the Canary basin (Fig. A.1 and Fig. A.2), with $f\text{CO}_{2,\text{sw}}$ values directly proportional ($R^2 > 0.76$) to the measured SST. Annual and seasonal average every 0.25° latitude (Fig. 5) showed that temperature drives $f\text{CO}_{2,\text{sw}}$ and FCO_2 variations. The maximum and minimum $f\text{CO}_{2,\text{sw}}$ and FCO_2 values were observed during summer (June-September) and winter (December-March), respectively. These values presented a strong latitudinal variability during all the seasons along the northwest African coastline. The average $f\text{CO}_{2,\text{sw}}$ and pH_T presented a maximum latitudinal variation during summer ($43.15 \pm 1.92 \mu\text{atm}$ and 0.036 ± 0.002 units, respectively), which was three times greater than the annual average of maximum latitudinal variation ($13.14 \pm 1.78 \mu\text{atm}$ and 0.011 ± 0.001 units, respectively).

Minimum summer average SST, SSS, $f\text{CO}_{2,\text{sw}}$ and FCO_2 and maximum summer pH_T were observed at the Cape Ghir latitude (Fig. 5), between the area of greatest intensity of the coastal upwelling to the north and the concave part of the coastline near the Canary archipelago, where the wind direction is locally modified and the upwelling is less intense.

Two anomalous events occurred on April 6 and December 14, 2019 (Fig. A.3): minimum and maximum values of $f\text{CO}_{2,\text{sw}}$, were respectively determined. At the same time, minimum SST were recorded in the section between Cape Sim (~31.4°N) and Beddouza (~32.5°N), possibly related to cold water upwelling. The minimum $f\text{CO}_{2,\text{sw}}$ on April 6, 2019 could indicate that

biological absorption reduced the CO₂ excess in cold upwelled waters, while the maximum in December suggests that biological activity at this time of the year was not enough to reduce the CO₂ excess.

Five stations were selected along the northwest African coast. The station at $29.8 \pm 0.2^\circ\text{N}$ (Fig. 6) is located near the Bay of Agadir, south of Cape Ghir, an area protected from strong north-easterly winds by the Atlas Mountains (Mittelstaedt, 1991). The stations at $30.7 \pm 0.2^\circ\text{N}$ (Fig. 6) and $31.2 \pm 0.2^\circ\text{N}$ (Fig. A.4) were located between Cape Ghir and Cape Sim and were used to study the influence of intense upwelling and the presence of a strong quasi-permanent filament on the CO₂ system and air-sea exchange at the longitude visited by the vessel. Finally, the stations at $33.0 \pm 0.2^\circ\text{N}$ (Fig. 6) and $34.2 \pm 0.2^\circ\text{N}$ (Fig. A.4) were located north of Cape Beddouza to compare the different influence of upwelling on the CO₂ system along the northwest African coast. Due to the longitudinal variability of the routes, westernmost and easternmost longitudinal intervals were represented separately to study the open-ocean and coastal waters, respectively.

The seasonal variation range of $f\text{CO}_{2,\text{sw}}$, pH_T and $\text{pH}_{\text{T},21}$ were maximum to the north of Cape Beddouza ($78.19 \pm 0.24 \mu\text{atm}$, 8.074 ± 0.001 and 0.046 ± 0.001 units, at station $33.0 \pm 0.2^\circ\text{N}$) and minimum around Cape Ghir ($49.47 \pm 0.03 \mu\text{atm}$, 8.048 ± 0.001 and 0.044 ± 0.001 units at station $30.7 \pm 0.2^\circ\text{N}$), coinciding with the maximum and minimum seasonal SST variation (6.43 ± 0.01 and 5.10 ± 0.05 °C at the respective stations). In the Bay of Agadir (Fig. 6), the SST, $f\text{CO}_{2,\text{sw}}$ and pH_T range was intermediate between those observed at the previous stations. The latitudinal difference was especially high during summer and autumn (Fig. 5) due to a spatial change in SST of ~ 3 °C (between ~ 20 and ~ 23 °C) throughout the latitudinal range, with maximum $f\text{CO}_{2,\text{sw}}$ and minimum pH_T around $420 \mu\text{atm}$ and 8.03 units, respectively, at the southernmost stations and $450 \mu\text{atm}$ and 8.01 - 8.02 units, respectively, at the northernmost stations (Fig. 5 and Fig. A.4). During winter and spring, the spatial change

in SST was slightly lower (~ 2 °C, between ~ 17 and ~ 19 °C) and the $f\text{CO}_{2,\text{sw}}$ and pH_T were practically constant at all stations (360-370 μatm and 8.08-8.09 units). The strongest sink was observed in the cold period between the Canary Islands and Cape Beddouza, where the range of variation of FCO_2 was maximum (between ~ -3.66 and ~ -1.46 $\text{mmol m}^{-2} \text{d}^{-1}$ south of Cape Beddouza and between ~ -2.35 and ~ -1.67 $\text{mmol m}^{-2} \text{d}^{-1}$ north of Cape Beddouza).

The T/B ratios (Table 2) show that the $f\text{CO}_{2,\text{sw}}$ variations were driven by thermal processes at all stations. The thermal effect on the seasonality of $f\text{CO}_{2,\text{sw}}$ was strongest north of Cape Beddouza towards more temperate regions, where the coastal upwelling loses intensity and biological activity is reduced. The lowest values (Table 2) were in Cape Ghir latitude, where the intensity of upwelling and phytoplankton blooms was highest. These differences derived from the change in the intensity of upwelling have also been reflected in the variation of C_T (Fig. A.5) which was maximum at $30.7 \pm 0.2^\circ\text{N}$ and $31.2 \pm 0.2^\circ\text{N}$, where the seasonal change in SSS (Fig. A.5) is greater due to the different intensity of the upwelling and offshore transport throughout the year. Once the salinity effect was removed, NC_T (Fig. A.5) decreased between February and October derived from the increase in biological uptake at this time of the year. Moreover, NC_T increases in the cold months due to both vertical mixing and the strong CO_2 sink at this time of year caused by the low SST recorded in the upwelling. At the rest of the stations, the variability of C_T and NC_T was lower and encompassed similar ranges to those observed on the inter-island routes, which reflects the lower influence of upwelling at these stations.

Longitudinal differences were observed between coastal and oceanic waters. The T/B ratio (Table 2) was higher in Cape Sim and Beddouza ($31.2 \pm 0.2^\circ\text{N}$ and $33.0 \pm 0.2^\circ\text{N}$, respectively), which may be related to the greater amplitude of seasonal variation in SST observed compared to the open-ocean zone.

4. Discussion

4.1. Seasonal variability of $f\text{CO}_{2,\text{sw}}$ and pH_{T}

The seasonal variability of $f\text{CO}_{2,\text{sw}}$ and FCO_2 values was driven by seasonal variations of SST, where the system behaved as a source in the warm months and as a sink in the cold months. This agrees with previous studies at the ESTOC site (González-Dávila et al., 2003; González-Dávila et al., 2010; Santana-Casiano et al., 2001; Santana-Casiano et al., 2007). The greatest increase in $f\text{CO}_{2,\text{sw}}$ occurred between winter and summer and followed a linear trend with temperature (Fig. A.6), with a linear regression slope of $12.27 \mu\text{atm } ^\circ\text{C}^{-1}$ for the GC-TNF route, $11.41 \mu\text{atm } ^\circ\text{C}^{-1}$ for the TNF-LNZ route and $11.71 \mu\text{atm } ^\circ\text{C}^{-1}$ for the CI-SG route. The theoretically $f\text{CO}_{2,\text{sw}} - \text{SST}$ relationship of $15.5 \pm 1.1 \mu\text{atm } ^\circ\text{C}^{-1}$ was reduced between February and October (10.35 , 9.81 and $10.48 \mu\text{atm } ^\circ\text{C}^{-1}$, respectively) as a consequence of the decrease in C_{T} due to biological drawdown. These results were slightly lower than those obtained between March and October for the ESTOC site ($12.12 \pm 0.48 \mu\text{atm } ^\circ\text{C}^{-1}$; González-Dávila et al., 2003). The seasonal variation of $f\text{CO}_{2,\text{sw}}$ led to a decrease in pH_{T} of 0.0009 units μatm^{-1} throughout the region between winter and summer, with an average variation range from 8.077 ± 0.007 to 8.037 ± 0.001 units in the Canary basin and from 8.084 ± 0.002 to 8.035 ± 0.002 units along the African coastline. The linear relationships between SST, $f\text{CO}_{2,\text{sw}}$ and pH_{T} at this time are presented in Table 3.

The T/B values (Table 2) indicate that the temperature effect on the CO_2 solubility in seawater controls air-sea exchange fluxes over biological uptake and other non-thermal processes. The contribution of the thermal processes in the variation of $f\text{CO}_{2,\text{sw}}$ was double the contribution of the biological activity at all the selected stations, with minimum T/B values higher than 1.60. Lowest values were obtained in the areas most influenced by the influx of nutrients and phytoplankton blooms, between Cape Sim and Cape Ghir, and with greater mesoscale variability south of Cape Ghir and at certain stations of the Canary archipelago.

4.2. Spatial variability of the CO₂ system parameters and fluxes

The differences observed in the seasonal variation for each carbon variable in the Canary basin and along the northwest African coastline are related to the hydrographic characteristics of each zone, to the intensity of the African coastal upwelling and to the mesoscale variability associated with offshore transport by filaments and eddies. The inter-island routes (GC-TNF-LNZ) presented differences between the oceanic and coastal waters. Seasonal variation of the CO₂ system and air-sea exchange were similar at $15.7 \pm 0.1^\circ\text{W}$ (GC-TNF), $15.6 \pm 0.1^\circ\text{W}$, $15.0 \pm 0.1^\circ\text{W}$ and $14.5 \pm 0.1^\circ\text{W}$ (TNF-LNZ) (Fig. 3 and Fig. 4). These stations were located in an open-ocean area directly exposed to the Canary Current and trade winds and protected from the filament incursion by the easternmost islands, Lanzarote and Fuerteventura (Davenport et al., 1999). However, the greatest $f\text{CO}_2$ variations occurred at the coastal stations due to higher differences in SST. The station at $16.05 \pm 0.1^\circ\text{W}$ (GC-TNF, Fig. 3) leeward of Tenerife presented higher average SST and SSS than those in open-ocean waters. At the station located within the Lanzarote-Fuerteventura channel ($13.9 \pm 0.1^\circ\text{W}$, Fig. 4), frequently influenced by coastal upwelling of cold-water and high-productivity filament incursion, the average SST and SSS were lower than in western waters throughout the year. A west to east decrease in $f\text{CO}_{2,\text{sw}}$ seasonal variability was observed in Canary Islands waters and in the T/B ratio on both inter-island routes. This shows that the thermal effect on $f\text{CO}_{2,\text{sw}}$ variability was greater in the westernmost section of each route, although clearly dominating in the entire Canary Islands subregion. The spatial variability was due to the recirculation of coastal upwelling in the Canary basin (Johnson and Stevens, 2000; Mittelstaedt, 1991; Pelegrí et al., 2005). The Canary Current diverges from the coast to the south of Cape Ghir and flows through the Canary archipelago. The majority of the flux travels between the eastern island channels, Gran Canaria-Fuerteventura and Fuerteventura-African coast (Hernández-Guerra et al., 2002; Knoll et al., 2002). This lead to the maximum CO₂ sink of the inter-island routes

observed at the easternmost stations of the TNF-LNZ route (between -0.32 ± 0.05 and -0.36 ± 0.04 mol m⁻² yr⁻¹, Fig. 4). The interaction between the Canary Current with the Cape Ghir filament, which extends beyond 15°W, forms cyclonic eddies which move southward, passing through the Canary Islands (Mittelstaedt, 1991). The recirculation results in the low SST and SSS signals observed between Gran Canaria and Tenerife from September to October, when the Cape Ghir filament was strongest. Evidence of upwelling has been observed on the west coast of Gran Canaria (Johnson and Stevens, 2000). This upwelling could produce the low T/B ratio (1.60) at the station located to the northwest of Gran Canaria ($15.7 \pm 0.1^\circ\text{W}$; GC-TNF).

The seasonal variation of the results along the continental shelf of northwest Africa presented an important latitudinal variation (Borges et al., 2005; Cui et al., 2006) related to the increase in the seasonal SST gradient towards higher latitudes from the Canary Islands to the Strait of Gibraltar. Regional differences in seawater properties along the African coastal transition zone are driven by the north-easterly winds and by the intensity of the permanent coastal upwelling between Cape Blanc and the Gulf of Cadiz. The mesoscale features were mainly generated by thermohaline horizontal gradients and by the dynamic character of the front from the coastal upwelling (Pastor et al., 2008; Pérez-Rodríguez et al., 2001; Zenk et al., 1991). These mesoscale features interacted with other mesoscale features, such as coastal cyclonic and anticyclonic eddies (Benítez-Barrios et al., 2011; Ruiz et al., 2014) which propagate westward as Rossby waves (Mason et al., 2011; Sangrà et al., 2009). These features promote the transport of the characteristics of the upwelling towards the open ocean in this Northeast Atlantic region (Valdés and Déniz-González, 2015).

The lowest SST, $f\text{CO}_{2,\text{sw}}$, FCO_2 and pH_T seasonal variability occurred at latitudes $30.7 \pm 0.2^\circ\text{N}$ (Fig. 6) and $31.2 \pm 0.2^\circ\text{N}$ (Fig. A.4) between Cape Ghir and Cape Beddouza. This region is characterised by a permanent and intense upwelling and offshore transport by

filaments, especially during summer (Johnson and Stevens, 2000; Mittelstaedt, 1991; Pelegrí et al., 2005). Near Cape Ghir ($\sim 30.6^\circ\text{N}$), a quasi-permanent surface filament is formed which stretches over 100 kilometres in open ocean (Hagen et al., 1996; Pelegrí et al., 2005) and is associated with the formation of cyclonic eddies to the south which are transported offshore (Johnson and Stevens, 2000). A detailed study of the Northwest African upwelling area provided by Mittelstaedt (1991) shows that upwelling is less intense throughout the year to the North of Cape Beddouza due to the concave shape of the Moroccan coastline to the Strait of Gibraltar and its unfavourable orientation against the equatorward blowing trades. It is more intense throughout the year between Cape Ghir and Beddouza, where the coastline has a convex shape and is more exposed to trade winds and the Canary Current. This explains that the annual and summer average of SST and SFS north of 33.0°N were higher than the values obtained at the Cape Ghir latitude. This local decrease in upwelling intensity caused a spatial variation of the CO_2 system and air-sea fluxes to the north of Cape Beddouza, where maximum annual and summer average of $f\text{CO}_{2,\text{sw}}$ and FCO_2 and minimum summer average of pH_T were observed.

The intensity of the upwelling in this region would also explain the fact that the minimum values of the T/B ratio along the African coastline were obtained at the stations of the greatest nutrient inflow and biological activity. The maximum T/B ratios (Table 2) were recorded north of Cape Beddouza, where the upwelling is less intense throughout the year. However, FCO_2 presented greater seasonality at latitudes $30.7 \pm 0.2^\circ\text{N}$ and $31.2 \pm 0.2^\circ\text{N}$, where the CO_2 sink expressed per unit area (-0.71 ± 0.04 and $-0.62 \pm 0.05 \text{ mol m}^{-2} \text{ yr}^{-1}$, respectively) was greater than north of Cape Beddouza ($-0.41 \pm 0.03 \text{ mol m}^{-2} \text{ yr}^{-1}$ for $33.0 \pm 0.2^\circ\text{N}$ and $-0.26 \pm 0.03 \text{ mol m}^{-2} \text{ yr}^{-1}$ for $34.2 \pm 0.2^\circ\text{N}$) and in the Bay of Agadir ($-0.51 \pm 0.04 \text{ mol m}^{-2} \text{ yr}^{-1}$; $29.8 \pm 0.2^\circ\text{N}$) (Fig. 6 and Fig. A.4). Moreover, this CO_2 sink was approximately twice that obtained in the Canary basin, which is less than $-0.36 \text{ mol m}^{-2} \text{ yr}^{-1}$ at all stations. The longitudinal

variability of the results, observable near Cape Sim and Beddouza, was related to seasonal differences in offshore transport and to the increase in SST and SSS from the coastal upwelling to open-ocean waters of $\sim 3.9^{\circ}\text{C}$ and ~ 0.2 units, respectively, estimated by Pelegrí et al. (2005). This contrasts with the homogeneous variation of $f\text{CO}_{2,\text{sw}}$ in waters close to the Cape Ghir latitude (Valdés and Déniz-González, 2015).

The $f\text{CO}_{2,\text{sw}}$ values obtained were compared and contextualized with the $f\text{CO}_{2,\text{sw}}$ data collected in SOCAT for the Northeast Atlantic referenced to the year 2019. The inclusion of SOCAT data is useful to understand the longitudinal change in $f\text{CO}_{2,\text{sw}}$ from coastal to open-ocean waters and to evaluate the representativeness of the results obtained by the CanOA-VOS line in a greater area in the Northeast Atlantic. Both data sets were studied as a function of longitude and time in the Canary archipelago (Fig. A.7) and in the 5 latitudes of interest along the northwest African coast (Fig 7 and A.8). SOCAT data show that the $f\text{CO}_{2,\text{sw}}$ surface longitudinal gradient is only significant in the first $0.5\text{-}1^{\circ}$ of longitude from the African coastline in the area of maximum upwelling ($30.7 \pm 0.2^{\circ}\text{N}$, Fig. 7; $31.2 \pm 0.2^{\circ}\text{N}$, Fig. A.8) and that it decreases towards the open ocean. This longitudinal gradient was clearly visible in the $f\text{CO}_{2,\text{sw}}$ data collected in coastal waters around Cape Ghir in April (CanOA-VOS) and September (SOCAT). The average $f\text{CO}_{2,\text{sw}}$ in April around $10.35 \pm 0.1^{\circ}\text{W}$ ($372.45 \pm 1.93 \mu\text{atm}$) was $\sim 9.5 \mu\text{atm}$ lower than that obtained around $11.5 \pm 0.2^{\circ}\text{W}$ ($381.97 \pm 4.22 \mu\text{atm}$). This longitudinal change was more drastic in September due to the strong upwelling at this time of the year that was visible in satellite SST data and because the SOCAT data was collected closer to the coast. The low $f\text{CO}_{2,\text{sw}}$ values obtained near the coast from SOCAT (Fig. 7) contrast with the maximum values of the annual cycle of $f\text{CO}_{2,\text{sw}}$ obtained by the CanOA-VOS towards open-ocean waters during late summer (Fig 5 and A.3). The average $f\text{CO}_{2,\text{sw}}$ in September around $10.15 \pm 0.2^{\circ}\text{W}$ ($376.64 \pm 14.28 \mu\text{atm}$) was $\sim 44 \mu\text{atm}$ lower than that obtained around $11.55 \pm 0.25^{\circ}\text{W}$ ($420.86 \pm 8.91 \mu\text{atm}$). These results show that there is a

significant longitudinal variation of $f\text{CO}_{2,\text{sw}}$ that changes with seasonality towards open-ocean waters in the first ~150 km from the Cape Ghir coastline. This longitudinal change does not appreciably affect the rest of the usual CanOA-VOS trips, which take place at a distance greater than 200 km from Cape Ghir. North of Cape Beddouza ($33.0 \pm 0.2^\circ\text{N}$ and $34.2 \pm 0.2^\circ\text{N}$, Fig. A.8) and south of Cape Ghir ($29.8 \pm 0.2^\circ\text{N}$, Fig. A.8) the longitudinal gradient is weaker due to the decrease in the intensity of the upwelling and values were not longitudinally modified.

In the easternmost part of the Canary archipelago (13-16°W), the $f\text{CO}_2$ values of CanOA-VOS line and SOCAT (Fig A.7) increased towards the west, driven by the east to west increase of SST throughout the year (Fig 2, A. 1, and A. 2), and in SST satellite images for the area. Data from SOOP CanOA-VOS improved the SOCAT v2020 data resolution for the area and showed the influence of mesoscale variations on the spatial distribution of $f\text{CO}_{2,\text{sw}}$ in the eastern part of the archipelago.

The seasonality of measured $f\text{CO}_{2,\text{sw}}$ values and its latitudinal variation was evaluated together with the SOCAT values in 3 areas of interest: the Canary archipelago ($27.5\text{-}29^\circ\text{N}$, Fig. A.9), Cape Ghir (30.7 , Fig 7) and North of Cape Beddouza ($33.0 \pm 0.2^\circ\text{N}$, Fig. A.9). The temporal distribution of the CanOA-VOS and SOCAT data were fitted to the harmonic equations in Table A.2. The SOCAT data collected in September in coastal waters of Cape Ghir have been excluded from the fitting to attend to the $f\text{CO}_{2,\text{sw}}$ seasonality in more open-ocean waters (Fig. 7). The $f\text{CO}_{2,\text{sw}}$ seasonality obtained from the CanOA-VOS database increased towards the North and was similar to that obtained from the SOCAT data in all areas, despite the SOCAT data having a greater longitudinal dispersion towards open ocean up to 20°W . This shows that even when there is a strong longitudinal gradient near the coast, at the location of the CanOA-VOS line the seasonality obtained was representative for a larger area in the Northeast Atlantic.

4.3. The relative contribution of biological activity, air-sea fluxes and horizontal transport to NC_T depletion

The temporal variation of C_T was studied in detail at the stations of the inter-island routes $15.7 \pm 0.1^\circ W$ (GC-TNF) and $14.5 \pm 0.1^\circ W$ (TNF-LNZ) located to the northwest of Gran Canaria and Fuerteventura, respectively, and at all selected stations on the African continental shelf. Previous CO_2 system studies in the surface ocean agree that the surface variation of C_T is mainly controlled by the factors which govern salinity and other non-conservative processes (i.e. primary production, oxidation of organic matter, precipitation and dissolution of calcium carbonate and air-sea CO_2 exchange) (e.g. Chen and Pytkowicz, 1979; Lee et al., 2000; Takahashi et al., 1993; Wanninkhof and Feely, 1998). In this study, C_T was normalised to a constant salinity of 36.7. The results allow to establish the relative importance of the air-sea exchange, the horizontal transport from the African coastal upwelling and the biological activity in the variability of NC_T between February and October. During this period, NC_T decreases and the vertical mixing is suppressed due to the decrease of the MLD, as estimated in the ESTOC site (Santana-Casiano et al., 2007) from ~ 120 meters (February-March) to ~ 25 meters (September-October). Near the northwest African coast, the contribution of vertical diffusion, advection and entrainment from the mixed layer due to the upwelling contributed to the NC_T variability. However, these processes were not accounted for due to the lack of data.

The monthly changes in NC_T by each of the terms in Eq. 8 were computed for the March-June, June-September and February-October periods (Fig. 8, Table 4). NC_T decreased from March-April to September-October and increased from November to March, driven by the biological activity and vertical mixing, with maximum primary production and respiration in the respective periods. Between February and October, a net decrease in NC_T was computed throughout the covered region, which was maximum at $31.2 \pm 0.2^\circ N$ ($-27.06 \text{ mmol m}^{-3}$) and

minimum at $29.8 \pm 0.2^\circ\text{N}$ ($-8.28 \text{ mmol m}^{-3}$). The variation of NC_T due to biological processes and calcification/dissolution represented $>90\%$ of $\Delta\text{NC}_T/\text{dt}$ at all stations between February and October. The effect of the air-sea exchange resulted in a net decrease in NC_T of $<6\%$. The greatest contribution of air-sea fluxes was observed at the stations located between Cape Ghir and Beddouza ($\sim 5.9\%$ at $30.7 \pm 0.2^\circ\text{N}$ and $\sim 2.77\%$ at $31.2 \pm 0.2^\circ\text{N}$) and within the Canary basin ($\sim 2.65\%$ at point $15.7 \pm 0.1^\circ\text{W}$ and $\sim 2.57\%$ at point $14.5 \pm 0.1^\circ\text{W}$), where the seasonal variation of FCO_2 was greater. The NC_T change induced by air-sea exchange was higher (between ~ -1.07 and $\sim -2.67 \text{ mmol m}^{-3}$) during summer (June-September), coinciding with the maximum outgassing period and greater stratification of the water column (González-Dávila et al., 2003; Santana-Casiano et al., 2007).

The CO_2 outgassing between June and September contributed between 12% and 20% in the depletion of NC_T in the entire region. However, at the northernmost station the contribution was minimal ($-0.67 \text{ mmol m}^{-3}$; $\sim 4.81\%$). The period between March and June presents the maximum primary production and change in sea surface behaviour from sink to source of CO_2 . During these months, the partial contribution of biological activity was higher than during summer and inversely for the air-sea exchange. However, these NC_T variation patterns presented differences between the stations. The lowest decrease in NC_T from February to October and from March to June were obtained in the most western transects around Bay of Agadir ($29.8 \pm 0.2^\circ\text{N}$) (Fig. 8), less influenced by coastal upwelling. At this location during spring, the air-sea exchange contributed 36.44% to the NC_T depletion, while the net community production represented 64.01%. The increase in the role of the air-sea exchange was due to the maximum CO_2 outgassing. Moreover, during this season, the upwelling and offshore transport by filaments is less intense in the Bay of Agadir (Mittelstaedt, 1991; Pelegrí et al., 2005). Therefore, the biological activity at the Bay of Agadir reduces faster towards the open ocean than at the higher latitudes of Cape Ghir and Cape Sim.

Differences in the contribution of the net community production were observed within the Canary basin, with a second sub-maximum in June-July. At $14.7 \pm 0.1^\circ\text{W}$, this was even higher than the first in April-June. The second maximum during June-July may be related to the strong biological activity associated with the maximum intensity of the Cape Ghir filament, as it is transported south by the recirculation of the Canary Current through the Canary archipelago (Hernández-Guerra et al., 2002; Knoll et al., 2002).

The contribution of the advection, transport and horizontal mixing processes to the NC_T depletion (Eq. 8) was calculated at the stations of the Canary basin, taking into account the difference in NC_T and SSS with respect to the most coastal station located at $30.7 \pm 0.2^\circ\text{N}$, in Cape Ghir latitude. Along the northwest African coast west-to-east gradients were performed considering the differences in values between the most oceanic and coastal stations. The greatest contribution occurred at $15.7 \pm 0.1^\circ\text{W}$ (Fig. 8) as a result of the greater difference in salinity between the more saline transition waters of the Canary archipelago and the less saline waters of the upwelling. Between February and October, the horizontal advection at this location increased NC_T by 1.55 mmol m^{-3} (~15%), with the highest increase during summer due to the greatest intensity of the upwelling (1.28 mmol m^{-3} , ~19%). At the other stations close to the African coast, NC_T and SSS gradients were close to zero and the horizontal transport contribution ranged between -0.49 and 0.33 mmol m^{-3} , contributing with <3.3%. These results coincide with those obtained in surface waters at the ESTOC site (González-Dávila et al., 2003) and provide a new estimation of the horizontal transport contribution of the coastal upwelling to the total NC_T change.

4.4. FCO_2 in the Northeast Atlantic coastal and transition region

The monitored routes presented annual negative values of FCO_2 and behaved as a net CO_2 sink. The spatial variation of FCO_2 was driven by the difference between $f\text{CO}_{2,\text{atm}}$ and $f\text{CO}_{2,\text{sw}}$ ($\Delta f\text{CO}_2$), since the wind speed did not present high variations between routes (Fig. 9). The

average FCO₂ calculated on the GC-TNF-LNZ routes was $-0.26 \pm 0.04 \text{ mol C m}^{-2} \text{ yr}^{-1}$, slightly higher than the average annual FCO₂ obtained at the ESTOC site between 1996 and 2000 ($-0.18 \text{ mol C m}^{-2} \text{ year}^{-1}$; González-Dávila et al., 2003). The annual average FCO₂ between Tenerife and Lanzarote (14,500 km² covered by the VOS line) was $-0.17 \pm 0.02 \text{ Tg CO}_2 \text{ yr}^{-1}$ ($\text{Tg}=10^{12} \text{ g}$) ($-0.05 \pm 0.01 \text{ Tg C yr}^{-1}$). The CO₂ sink in the Canary basin was half of what was determined along the northwest African coast ($-0.48 \pm 0.09 \text{ mol C m}^{-2} \text{ yr}^{-1}$). For the northwest African coast covered by the VOS line from 28.9°N to 35.8°N (160,500 km²), an annual average FCO₂ of $-3.36 \pm 0.61 \text{ Tg CO}_2 \text{ yr}^{-1}$ ($-0.92 \pm 0.17 \text{ Tg C yr}^{-1}$) was computed. The average FCO₂ calculated for the entire study region (175,000 km²) was $-0.34 \pm 0.06 \text{ mol C m}^{-2} \text{ yr}^{-1}$, which is consistent with that obtained from SOCAT data ($-0.37 \pm 1.11 \text{ mol C m}^{-2} \text{ yr}^{-1}$) for a larger area (26-38°N, 5-20°W) in the Northeast Atlantic (1,200,000 km²). These values are lower than the carbon fluxes reported for the Northeast Atlantic ($-0.6 \text{ mol C m}^{-2} \text{ yr}^{-1}$, Takahashi et al., 2009) and for the continental shelf of the Northeast Atlantic ($-0.8 \text{ mol C m}^{-2} \text{ yr}^{-1}$, Chen and Borges, 2009). However, these later calculations were performed with limited datasets. The average FCO₂ for the entire study region was $-2.65 \pm 0.44 \text{ Tg CO}_2 \text{ yr}^{-1}$ ($-0.72 \pm 0.12 \text{ Tg C yr}^{-1}$). This result agrees with previous research indicating that the Northeast Atlantic ocean acts as an active CO₂ sink (e.g. Khatiwala et al., 2013; Leseurre et al., 2020; Sabine et al., 2004; Takahashi et al., 2009) and with the role of continental shelves (e.g. Borges et al., 2005; Cai, 2011; Chen et al., 2013).

5. Conclusion

The results obtained between February 2019 and February 2020 proved the seasonal and spatial variability of the CO₂ system parameters and fluxes in surface waters of the easternmost part of the Canary basin and on the northwest African continental shelf. The seasonal behaviour agrees with previous studies at the ESTOC site (González-Dávila et al., 2003; González-Dávila et al., 2010; Santana-Casiano et al., 2007), with the northwest African

coastal upwelling system (Pelegrí et al., 2005) and with North Atlantic global surface ocean studies (Takahashi et al., 2009). The temporal and spatial change of the variables was strongly driven by temperature fluctuations with the seasons. The effect increased with latitude and presented local differences due to varying intensities of the upwelling and offshore transport along the northwest African coastline. The lowest SST and SSS were registered in the region with the greatest intensity of upwelling, between Cape Ghir and Beddouza (~30.6-32.5°N) (Fig. 5) and in the areas most affected by offshore transport between the eastern islands of the Canary archipelago (~15.4-13.5°N) (Fig. 2). In these areas, the seasonal variation of $f\text{CO}_{2,\text{sw}}$ and pH_T were minimal ($42.47 \pm 0.03 \mu\text{atm}$ and 0.048 ± 0.001 units, calculated at station $30.7 \pm 0.2^\circ\text{N}$) due to the low values obtained during summer. The $f\text{CO}_{2,\text{sw}}$ increased on the inter-island routes by $10.68 \pm 0.22 \mu\text{atm } ^\circ\text{C}^{-1}$ from February to October, which led to a pH_T decrease of 0.001 units μatm^{-1} . On the northwest African continental shelf, the increase in $f\text{CO}_{2,\text{sw}}$ in the same period was $10.48 \pm 0.17 \mu\text{atm } ^\circ\text{C}^{-1}$ (a pH_T decrease of 0.0009 units μatm^{-1}). NC_T seasonality was driven first by net community production and second by air-sea exchange. It was highest in the areas of maximum upwelling with higher biological activity and seasonal variation of the air-sea CO_2 fluxes. The surface waters of the entire region acted as a CO_2 sink during the cold months and as a source during the warm months. The area between the Canary Islands (28.1°N) and the entry of the Strait of Gibraltar (35.8°N) presented an average CO_2 flux of $-2.65 \pm 0.44 \text{ Tg CO}_2 \text{ yr}^{-1}$ ($-0.72 \pm 0.12 \text{ Tg C yr}^{-1}$). The CO_2 sink was found to be maximum in Cape Ghir and throughout the area of maximum upwelling due to minimum temperatures throughout the year which favour the solubility of CO_2 in seawater. The CO_2 consumption by an increased productivity in the upwelling area was counteracted by the injection of rich CO_2 deep seawater, resulted in a depletion in both NC_T and $f\text{CO}_2$. The Canary archipelago, with higher annual temperatures, and the area north of Cape Beddouza, where the upwelling intensity

declines, were weak CO₂ sinks.

This study shows that high-frequency continuous monitoring of the CO₂ system by VOS lines is a powerful tool to study the carbon cycle in the global surface ocean. The results expand our knowledge of air-sea CO₂ exchange in the eastern boundary upwelling system of the North Atlantic subtropical gyre and highlight the importance of continuous high-temporal and spatial resolution data records. The inclusion of the CanOA-VOS line data in the SOCAT database provides a better understanding of the temporal and spatial distribution of CO₂ in the surface Northeast Atlantic Ocean and appreciably increases the monitored area, especially in inter-island waters of the Canary archipelago and in certain locations along the northwest African coast where no previous data had been obtained.

Acknowledgments

This study was supported by the Canary Islands Government and the Loro Parque Foundation through the CanBIO project, CanOA subproject (2019-2022) and the CARBOCAN agreement (Consejería de Transición Ecológica, Lucha contra el Cambio Climático y Planificación Territorial, Gobierno de Canarias). We would like to thank the RENATE P ship owner, the NISA-Marítima company and the captains and crew members for the support during this collaboration. Special thanks to the technician Adrian Castro-Alamo for biweekly equipment maintenance and discrete sampling of total alkalinity aboard the ship. The VOS line will be part of the Spanish contribution to the Integrated Carbon Observation System, ICOS, European Research Infrastructure starting in 2021. This study was completed while D.C.-H. was a Master student in the Oceanography and Global Change program at the Faculty of Marine Science, Universidad de Las Palmas de Gran Canaria. We thank the Surface Ocean CO₂ Atlas (SOCAT), an international effort, endorsed by the International Ocean Carbon Coordination Project (IOCCP), the Surface Ocean Lower Atmosphere Study (SOLAS) and the Integrated Marine Biosphere Research (IMBeR) program, to deliver a

uniformly quality-controlled surface ocean CO₂ database. The many researchers and funding agencies responsible for the collection of data and quality control are thanked for their contributions to SOCAT.

Author contribution

All authors made significant contributions towards the writing of the manuscript. M.G.-D., J. M. S.-C. and A.G.G. installed and maintained the equipment in the VOS line. D. C.-H. and D. G.-S. performed the data treatments and MATLAB[®] routines.

References

- Bates, N.R., Astor, Y.M., Church, M.J., Currie, K., Dore, J.E., González-Dávila, M., Lorenzoni, L., Muller-Karger, F., Olafsson, J., and Santana-Casiano, J.M. (2014). A time-series view of changing ocean chemistry due to ocean uptake of anthropogenic CO₂ and ocean acidification. *Oceanography*, 27(1), 126–141, <http://dx.doi.org/10.5670/oceanog.2014.16>.
- Benítez-Barrios, V. M., Pelegrí, J. L., Hernández-Guerra, A., Lwiza, K. M. M., Gomis, D., Vélez-Belchí, P., and Hernández León, S. (2011). Three-dimensional circulation in the NW Africa coastal transition zone. *Progress in Oceanography*, 91(4), 516–533. <https://doi.org/10.1016/j.procean.2011.07.022>
- Borges, A. V., Delille, E. and Frankignoulle, M. (2005). Budgeting sinks and sources of CO₂ in the coastal ocean: Diversity of ecosystem counts. *Geophysical Research Letters*, 32(14), 1–4. <https://doi.org/10.1029/2005GL023053>
- de Boyer Montégut, C., Madec, G., Fischer, A.S., Lazar, A., Iudicone, D., (2004). Mixed layer depth over the global ocean: An examination of profile data and a profile-based climatology. *Journal of Geophysical Research: Oceans*. 109, 1–20. <https://doi.org/10.1029/2004JC002378>
- de Boyer Montégut, C., Mignot, J., Lazar, A., Cravatte, S., (2007). Control of salinity on the

- mixed layer depth in the world ocean: 1. General description. *Journal of Geophysical Research: Oceans*. 112, 1–12. <https://doi.org/10.1029/2006JC003953>
- Brainerd, K. E., and Gregg, M. C. (1995). Surface mixed and mixing layer depths. *Deep-Sea Research Part I*, 42(9), 1521–1543. [https://doi.org/10.1016/0967-0637\(95\)00068-H](https://doi.org/10.1016/0967-0637(95)00068-H)
- Cai, W. J. (2011). Estuarine and coastal ocean carbon paradox: CO₂ sinks or sites of terrestrial carbon incineration? *Annual Review of Marine Science*, 3, 123–145. <https://doi.org/10.1146/annurev-marine-120709-142723>
- Cai, W. J., Dai, M., and Wang, Y. (2006). Air-sea exchange of carbon dioxide in ocean margins: A province-based synthesis. *Geophysical Research Letters*, 33(12). <https://doi.org/10.1029/2006GL026219>
- Chen, T. A., Huang, T. H., Chen, Y. C., Bai, Y., He, X., and Kang, Y. (2013). Air-sea exchanges of coin the world's coastal seas. *Biogeosciences*, 10(10), 6509–6544. <https://doi.org/10.5194/bg-10-6509-2013>
- Chen, T. A., and Pytkowicz, R. M. (1979). On the total CO₂-titration alkalinity-Oxygen system in the Pacific Ocean. *Nature*, 281, 362–365. <https://doi.org/10.1038/281362a0>
- Chen, T. A., and Borges, A. V. (2009). Reconciling opposing views on carbon cycling in the coastal ocean: Continental shelves as sinks and near-shore ecosystems as sources of atmospheric CO₂. *Deep-Sea Research Part II: Topical Studies in Oceanography*, 56(8–10), 578–590. <https://doi.org/10.1016/j.dsr2.2009.01.001>
- Davenport, R., Neuer, S., Hernandez-Guerra, A., Rueda, M. J., Llinas, O., Fischer, G., and Wefer, G. (1999). Seasonal and interannual pigment concentration in the Canary Islands region from CZCS data and comparison with observations from the ESTOC. *International Journal of Remote Sensing*, 20(7), 1419–1433. <https://doi.org/10.1080/014311699212803>
- Dickson, A. G. (1990). Standard potential of the reaction: AgCl(s) + 1/2H₂(g) = Ag(s) +

- HCl(aq) and the standard acidity constant of the ion HSO_4^- in synthetic sea water from 273.15 to 318.15 K. *The Journal of Chemical Thermodynamics*, 22(2), 113–127.
[https://doi.org/10.1016/0021-9614\(90\)90074-Z](https://doi.org/10.1016/0021-9614(90)90074-Z)
- Dickson, A. G., Sabine, C. L. and Christian, J. R. (2007). Guide to Best Practices for Ocean CO_2 Measurements. PICES Special Publication 3, 191 pp.
- Doney, S. C., Fabry, V. J., Feely, R. A., and Kleypas, J. A. (2009). Ocean Acidification: the other CO_2 problem. *Annual Review of Marine Science*, 1(1), 169–192.
<https://doi.org/10.1146/annurev.marine.010908.163834>
- Feely, R. A., Wanninkhof, R., Milburn, H. B., Cosca, C. E., Stapp, M., and Murphy, P. P. (1998). A new automated underway system for making high precision pCO_2 measurements onboard research ships. *Analytica Chimica Acta*, 377(2–3), 185–191.
[https://doi.org/10.1016/S0003-2670\(98\)00353-2](https://doi.org/10.1016/S0003-2670(98)00353-2)
- Frankignoulle, M., and Borges, A. V. (2001). European continental shelf as a significant sink for atmospheric carbon dioxide. *Global Biogeochemical Cycles*, 15(3), 569–576.
<https://doi.org/10.1029/2000GB001307>
- Friedlingstein, P., Jones, M. W., O'Sullivan, M., Andrew, R. M., Hauck, J., Peters, G. P., Peters, W., Pongratz, J., Schaefer, S., Quéré, C., Bakker, D. C. E., Canadell, J. G., Ciais, P., Jackson, R. B., Arndt, P., Barbero, L., Bastos, A., Bastrikov, V., Becker, M., Bopp, L., Buitenhuis, E., Chandra, N., Chevallier, F., Chini, L. P., Currie, K. I., Feely, R. A., Gehlen, M., Gilfillan, D., Gkritzalis, T., Goll, D. S., Gruber, N., Gutekunst, S., Harris, I., Havard, V., Houghton, R. A., Hurtt, G., Ilyina, T., Jain, A. K., Joetzjer, E., Kaplan, J. O., Kato, E., Klein Goldewijk, K., Korsbakken, J. I., Landschützer, P., Lauvset, S. K., Lefèvre, N., Lenton, A., Lienert, S., Lombardozzi, D., Marland, G., McGuire, P. C., Melton, J. R., Metzl, N., Munro, D. R., Nabel, J. E. M. S., Nakaoka, S., Neill, C., Omar, A. M., Ono, T., Peregon, A., Pierrot, D., Poulter, B., Rehder, G., Resplandy, L.,

- Robertson, E., Rödenbeck, C., Séférian, R., Schwinger, J., Smith, N., Tans, P. P., Tian, H., Tilbrook, B., Tubiello, F. N., Van der Werf, G. R., Wiltshire, A. J., and Zaehle, S. (2019). Global Carbon Budget 2019. *Earth System Science Data*, 11(4), 1783–1838. <https://doi.org/10.5194/essd-11-1783-2019>
- Gattuso, J.P., and Hansson, L. (2011). *Ocean Acidification*, Oxford University Press, 352 pp.
- González-Dávila, M., Santana-Casiano, J. M., Rueda, M. J., and Llinás, O. (2010). The water column distribution of carbonate system variables at the ESTOC site from 1995 to 2004. *Biogeosciences*, 7(10), 3067–3081. <https://doi.org/10.5194/bg-7-3067-2010>
- González-Dávila, M., Santana-Casiano, J. M., Rueda, M.J., Llinás, O., and González-Dávila, E. F. (2003). Seasonal and interannual variability of sea-surface carbon dioxide species at the European Station for Time Series in the Ocean at the Canary Islands (ESTOC) between 1996 and 2000. *Global Biogeochemical Cycles*, 17(3), 1076. <https://doi.org/10.1029/2002gb001993>
- Gruber, N., Clement, D., Carter, B. R., Feely, R. A., van Heuven, S., Hoppema, M., Ishii, M., Key, R. M., Kozyr, A., Lauvset, S. K., Lo Monaco, C., Mathis, J. T., Murata, A., Olsen, A., Pérez, F. F., Sabine, C. L., Tanhua, T., and Wanninkhof, R. (2019). The oceanic sink for anthropogenic CO_2 from 1994 to 2007. *Science*, 363(6432), 1193–1199. <https://doi.org/10.1126/science.aau5153>
- Gruber, N., Keeling, C. D., and Stocker, T. F. (1998). Carbon-13 constraints on the seasonal inorganic carbon budget at the BATS site in the Northwestern Sargasso Sea. *Deep-Sea Research Part I: Oceanographic Research Papers*, 45(4–5), 673–717. [https://doi.org/10.1016/S0967-0637\(97\)00098-8](https://doi.org/10.1016/S0967-0637(97)00098-8)
- Hagen, E., Züllicke, C., and Feistel, R. (1996). Near-surface structures in the Cape Ghir filament off Morocco. *Oceanologica Acta*, 19(6), 577-598.
- Hernández-Guerra, A., Machín, F., Antoranz, A., Cisneros-Aguirre, J., Gordo, C., Marrero-

- Díaz, A., Martínez, A., Ratsimandresy, A.W., Rodríguez-Santana, A., Sangrá, P., López-Laazen, F., Parrilla, G., and Pelegrí, J. L. (2002). Temporal variability of mass transport in the Canary Current. *Deep-Sea Research Part II: Topical Studies in Oceanography*, 49(17), 3415–3426. [https://doi.org/10.1016/S0967-0645\(02\)00092-9](https://doi.org/10.1016/S0967-0645(02)00092-9)
- Huntsman, S. A., and Barber, R. T. (1977). Primary production off northwest Africa: the relationship to wind and nutrient conditions. *Deep-Sea Research*, 24(1), 25–33. [https://doi.org/10.1016/0146-6291\(77\)90538-0](https://doi.org/10.1016/0146-6291(77)90538-0)
- Jewell, P. W. (1994). Mass balance models of Ekman Transport and nutrient fluxes in coastal upwelling zones. *Global Biogeochemical Cycles*, 8(2), 165–177. <https://doi.org/10.1029/94GB00097>
- Jing, Y., Li, Y., Xu, Y., and Fan, G. (2019). Influence of the NAO on the North Atlantic CO₂ fluxes in winter and summer on the interannual scale. *Advances in Atmospheric Sciences*, 36(11), 1288–1298. <https://doi.org/10.1007/s00376-019-8247-2>
- Johnson, J., and Stevens, I. (2000). A fine resolution model of the eastern North Atlantic between the Azores, the Canary Islands and the Gibraltar Strait. *Deep-Sea Research Part I: Oceanographic Research Papers*, 47(5), 875–899. [https://doi.org/10.1016/S0967-0637\(99\)00073-4](https://doi.org/10.1016/S0967-0637(99)00073-4)
- Khatiwala, S., Tanhua, T., Mikaloff Fletcher, S., Gerber, M., Doney, S. C., Graven, H. D., Gruber, N., McKinley, G. A., Murata, A., Ríos, A. F., and Sabine, C. L. (2013). Global ocean storage of anthropogenic carbon. *Biogeosciences*, 10(4), 2169–2191. <https://doi.org/10.5194/bg-10-2169-2013>
- Knoll, M., Hernández-Guerra, A., Lenz, B., López Laatzén, F., Machín, F., Müller, T. J., and Siedler, G. (2002). The Eastern Boundary Current system between the Canary Islands and the African Coast. *Deep-Sea Research Part II: Topical Studies in Oceanography*, 49(17), 3427–3440. [https://doi.org/10.1016/S0967-0645\(02\)00105-4](https://doi.org/10.1016/S0967-0645(02)00105-4)

- Lee, K., Kim, T. W., Byrne, R. H., Millero, F. J., Feely, R. A., and Liu, Y. M. (2010). The universal ratio of boron to chlorinity for the North Pacific and North Atlantic oceans. *Geochimica et Cosmochimica Acta*, 74(6), 1801–1811. <https://doi.org/10.1016/j.gca.2009.12.027>
- Lee, K., Tong, L. T., Millero, F. J., Sabine, C. L., Dickson, A. G., Goyet, C., Park, P., Wanninkhof, R., Feely, R. A., and Key, R. M. (2006). Global relationships of total alkalinity with salinity and temperature in surface waters of the world's oceans. *Geophysical Research Letters*, 33(19), 1–5. <https://doi.org/10.1029/2006GL027207>
- Lee, K., Wanninkhof, R., Feely, R. A., Millero, F. J., and Peng, T. H. (2000). Global relationships of total inorganic carbon with temperature and nitrate in surface seawater. *Global Biogeochemical Cycles*, 14(3), 979–994. <https://doi.org/10.1029/1998GB001087>
- Le Quéré, C., Andrew, R. M., Friedlingstein, P., Sitch, S., Hauck, J., Pongratz, J., Pickers, P. A., Korsbakken, J. I., Peters, G. P., Canadell, J. G., Arneeth, A., Arora, V. K., Barbero, L., Bastos, A., Bopp, L., Chevallier, F., Chini, L. P., Ciais, P., Doney, S. C., Gkritzalis, T., Goll, D. S., Harris, I., Havercorn, W., Hoffman, F. M., Hoppema, M., Houghton, R. A., Hurtt, G., Ilyina, T., Jain, A. K., Johannessen, T., Jones, C. D., Kato, E., Keeling, R. F., Goldewijk, K. K., Landolt, P., Lefèvre, N., Lienert, S., Liu, Z., Lombardozzi, D., Metzl, N., Munro, D. R., Nabel, J. E. M. S., Nakaoka, S., Neill, C., Olsen, A., Ono, T., Patra, P., Peregon, A., Peters, W., Peylin, P., Pfeil, B., Pierrot, D., Poulter, B., Rehder, G., Resplandy, L., Robertson, E., Rocher, M., Rödenbeck, C., Schuster, U., Schwinger, J., Séférian, R., Skjelvan, I., Steinhoff, T., Sutton, A., Tans, P. P., Tian, H., Tilbrook, B., Tubiello, F. N., van der Laan-Luijkx, I. T., van der Werf, G. R., Viovy, N., Walker, A. P., Wiltshire, A. J., Wright, R., Zaehle, S., and Zheng, B. (2018). Global Carbon Budget 2018. *Earth System Science Data*, 10, 2141–2194, <https://doi.org/10.5194/essd-10-2141-2018>, 2018, 2018

- Leseurre, C., Lo Monaco, C., Reverdin, G., Metzl, N., Fin, J., Olafsdottir, S., and Racapé, V. (2020). Ocean carbonate system variability in the North Atlantic Subpolar surface water (1993-2017). *Biogeosciences*, 17(9), 2553–2577. <https://doi.org/10.5194/bg-17-2553-2020>
- Lueker, T. J., Dickson, A. G., and Keeling, C. D. (2000). Ocean pCO₂ calculated from dissolved inorganic carbon, alkalinity, and equations for K₁ and K₂: Validation based on laboratory measurements of CO₂ in gas and seawater at equilibrium. *Marine Chemistry*, 70(1–3), 105–119. [https://doi.org/10.1016/S0304-4203\(00\)00022-0](https://doi.org/10.1016/S0304-4203(00)00022-0)
- Lüger, H., Wallace, D. W. R., Körtzinger, A., and Nojiri, Y. (2004). The pCO₂ variability in the midlatitude North Atlantic Ocean during a full annual cycle. *Global Biogeochemical Cycles*, 18(3), 3023. <https://doi.org/10.1029/2003GB002200>
- Mason, E., Colas, F., Molemaker, J., Shchepetkin, A. F., Troupin, C., McWilliams, J. C., and Sangrà, P. (2011). Seasonal variability of the Canary Current: A numerical study. *Journal of Geophysical Research: Oceans*, 116(6), 6001. <https://doi.org/10.1029/2010JC006565>
- Mignot, J., de Boyer Montégut, C., Lazar, A., Cravatte, S., 2007. Control of salinity on the mixed layer depth in the world ocean: 2. Tropical areas. *Journal of Geophysical Research: Oceans*, 112, 1–12. <https://doi.org/10.1029/2006JC003954>
- Mintrop, L., Pérez, F. F., González-Dávila, M., Santana-Casiano, J. M., and Körtzinger, A. (2000). Alkalinity determination by potentiometry: Intercalibration using three different methods. *Ciencias Marinas*, 26(1), 23–37. <https://doi.org/10.7773/cm.v26i1.573>
- Mittelstaedt, E. (1991). The ocean boundary along the northwest African coast: Circulation and oceanographic properties at the sea surface. *Progress in Oceanography*, 26(4), 307–355. [https://doi.org/10.1016/0079-6611\(91\)90011-A](https://doi.org/10.1016/0079-6611(91)90011-A)
- Pastor, M. V., Pelegrí, J. L., Hernández-Guerra, A., Font, J., Salat, J., and Emelianov, M.

- (2008). Water and nutrient fluxes off Northwest Africa. *Continental Shelf Research*, 28(7), 915–936. <https://doi.org/10.1016/j.csr.2008.01.011>
- Pelegrí, J. L., Arístegui, J., Cana, L., González-Dávila, M., Hernández-Guerra, A., Hernández-León, S., Marrero-Díaz, A., Montero, M. F., Sangrà, P., and Santana-Casiano, M. (2005). Coupling between the open ocean and the coastal upwelling region off northwest Africa: Water recirculation and offshore pumping of organic matter. *Journal of Marine Systems*, 54(1-4), 3–37. <https://doi.org/10.1016/j.jmarsys.2004.07.003>
- Pérez-Rodríguez, P., Pelegrí, J. L., and Marrero-Díaz, A. (2001). Dynamical characteristics of the Cape Verde frontal zone. *Scientia Marina*, 65, 241–250. <https://doi.org/10.3989/scimar.2001.65s1241>
- Pierrot, D., Neill, C., Sullivan, K., Castle, R., Wanninkhof, R., Lüger, H., Johannessen, T., Olsen, A., Feely, R. A., and Cosca, C. E. (2009). Recommendations for autonomous underway pCO₂ measuring systems and data-reduction routines. *Deep-Sea Research Part II: Topical Studies in Oceanography*, 56(8–10), 512–522. <https://doi.org/10.1016/j.dsr2.2008.12.005>
- Ruiz, S., Pelegrí, J. L., Emelianov, M., Pascual, A., and Mason, E. (2014). Geostrophic and ageostrophic circulation in a shallow anticyclonic eddy off Cape Bojador. *Journal of Geophysical Research: Oceans*, 119(2), 1257–1270. <https://doi.org/10.1002/2013JC009169>
- Sabine, C. L., Feely, R. A., Gruber, N., Key, R. M., Lee, K., Bullister, J. L., Wanninkhof, R., Wong, C. S., Wallace, D., Tilbrook, B., Millero, F. J., Peng, T., Kozyr, A., Ono, T., and Rios, A. F. (2004). The oceanic sink for anthropogenic CO₂. *Science*, 305(5682), 367–371. <https://doi.org/10.1126/science.1097403>
- Sangrà, P., Pascual, A., Rodríguez-Santana, Á., Machín, F., Mason, E., McWilliams, J. C., Pelegrí, J. L., Dong, C., Rubio, A. M., Arístegui, J., Marrero-Díaz, A., Hernández-

- Guerra, A., Martínez-Marrero, A., and Auladell, M. (2009). The Canary Eddy Corridor: A major pathway for long-lived eddies in the subtropical North Atlantic. *Deep-Sea Research Part I: Oceanographic Research Papers*, 56(12), 2100–2114. <https://doi.org/10.1016/j.dsr.2009.08.008>
- Santana-Casiano, J. M., González-Dávila, M., Laglera-Baquer, L. M., and Rodríguez-Somoza, M. J. (2001). Carbon dioxide system in the Canary region during October 1995. *Scientia Marina*, 65(S1), 41–49. <https://doi.org/10.3989/scimar.2001.65s141>
- Santana-Casiano, J. M., González-Dávila, M., Rueda, M. J., Llinás, O., and González-Dávila, E. F. (2007). The interannual variability of oceanic CO₂ parameters in the northeast Atlantic subtropical gyre at the ESTOC site. *Global Biogeochemical Cycles*, 21(1) 1015. <https://doi.org/10.1029/2006GB002788>
- Sarmiento, J. L., and Gruber, N., (2006). *Ocean Biogeochemical Dynamics*. Cambridge University.
- Shadwick, E. H., Thomas, H., Azetsu-Scott, K., Greenan, B. J. W., Head, E., and Horne, E. (2011). Seasonal variability of dissolved inorganic carbon and surface water pCO₂ in the Scotian Shelf region of the Northwestern Atlantic. *Marine Chemistry*, 124 (1-4), 23-37. <https://doi.org/10.1016/j.marchem.2010.11.004>
- Shadwick, E. H., Thomas, H., Comeau, A., Craig, S. E., Hunt, C. W., and Salisbury, J. E. (2010). Air-Sea CO₂ fluxes on the Scotian Shelf: seasonal to multi-annual variability. *Biogeosciences*, 7, 3851–3867. <https://doi.org/10.5194/bg-7-3851-2010>
- Takahashi, T., Olafsson, J., Goddard, J. G., Chipman, D. W., and Sutherland, S. C. (1993). Seasonal variation of CO₂ and nutrients in the high-latitude surface oceans: A comparative study. *Global Biogeochemical Cycles*, 7(4), 843–878. <https://doi.org/10.1029/93GB02263>
- Takahashi, T., Sutherland, S. C., Sweeney, C., Poisson, A., Metzl, N., Tilbrook, B., Bates, N.,

- Wanninkhof, R., Feely, R. A., Sabine, C., Olafsson, J., and Nojiri, Y. (2002). Global sea-air CO₂ flux based on climatological surface ocean pCO₂, and seasonal biological and temperature effects. *Deep-Sea Research Part II: Topical Studies in Oceanography*, 49(9–10), 1601–1622. [https://doi.org/10.1016/S0967-0645\(02\)00003-6](https://doi.org/10.1016/S0967-0645(02)00003-6)
- Takahashi, T., Sutherland, S. C., Wanninkhof, R., Sweeney, C., Feely, R. A., Chipman, D. W., Hales, B., Friederich, G., Chávez, F., Sabine, C., Watson, A., Bakker, D. C. E., Schuster, U., Metzl, N., Yoshikawa-Inoue, H., Ishii, M., Midorikawa, T., Nojiri, Y., Körtzinger, A., Steinhoff, T., Hoppema, M., Olafsson, J., Amarson, T. S., Tilbrook, B., Johannessen, T., Olsen, A., Bellerby, R., Wong, C. S., Delille, D., Bates, N. R., and de Baar, H. J. W. (2009). Climatological mean and decadal change in surface ocean pCO₂, and net sea-air CO₂ flux over the global oceans. *Deep-Sea Research Part II: Topical Studies in Oceanography*, 56(8–10), 554–577. <https://doi.org/10.1016/j.dsr2.2008.12.009>
- Valdés, L., and Déniz-González, I. (2015). Oceanographic and biological features in the Canary Current Large Marine Ecosystem. *IOC-UNESCO, Paris, IOC Techni*, 383.
- Wanninkhof, R. (2014). Relationship between wind speed and gas exchange over the ocean revisited. *Limnology and Oceanography: Methods*, 12(6), 351–362. <https://doi.org/10.4319/lom.2014.12.351>
- Wanninkhof, R., and Feely, R. A. (1998). fCO₂ dynamics in the Atlantic, South Pacific and South Indian oceans. *Marine Chemistry*, 60(1–2), 15–31. [https://doi.org/10.1016/S0304-4203\(97\)00088-1](https://doi.org/10.1016/S0304-4203(97)00088-1)
- Weiss, R. F., and Price, B. A. (1980). Nitrous oxide solubility in water and seawater. *Marine Chemistry*, 8(4), 347–359. [https://doi.org/10.1016/0304-4203\(80\)90024-9](https://doi.org/10.1016/0304-4203(80)90024-9)
- Zenk, W., Klein, B., and Schroder, M. (1991). Cape Verde Frontal Zone. *Deep Sea Research Part A. Oceanographic Research Papers*, 38, S505–S530.

[https://doi.org/10.1016/s0198-0149\(12\)80022-7](https://doi.org/10.1016/s0198-0149(12)80022-7)

Table 1. Annual and seasonal averages of SST, SSS, and CO₂ system parameters and fluxes with their respective standard deviations on the GC-TNF, TNF-LNZ and CI-SG routes.

		SST (°C)	SSS	C _T (μmol kg ⁻¹)	NC _T (μmol kg ⁻¹)	fCO _{2,s} w (μatm)	FCO ₂ (mmol m ⁻² d ⁻¹)	pH _T	pH _{T,21}
GC- TNF	Win ter	19.21 ± 0.02	36.796 ± 0.007	2114.5 5 ± 0.41	2109.1 8 ± 0.71	378.00 ± 0.58	-3.41 ± 0.08	8.077 ± 0.001	8.049 ± 0.001
	Spri ng	19.95 ± 0.04	36.730 ± 0.017	2114.9 5 ± 0.72	2113.0 5 ± 0.84	393.19 ± 0.95	-1.47 ± 0.13	8.064 ± 0.001	8.047 ± 0.001
	Su mm er	22.36 ± 0.04	36.796 ± 0.039	2107.0 1 ± 2.19	2101.7 1 ± 1.40	420.15 ± 0.58	2.15 ± 0.07	8.037 ± 0.001	8.057 ± 0.001
	Aut umn	22.01 ± 0.05	36.715 ± 0.019	2101.8 2 ± 0.94	2100.6 3 ± 1.08	402.83 ± 0.72	0.14 ± 0.13	8.052 ± 0.001	8.067 ± 0.001
	Ann ual	21.00 ± 0.04	36.754 ± 0.020	2108.7 0 ± 1.03	2105.5 7 ± 1.01	399.20 ± 0.73	-0.57 ± 0.11	8.057 ± 0.001	8.056 ± 0.001
TNF - LNZ	Win ter	19.10 ± 0.04	36.768 ± 0.009	2115.0 4 ± 0.53	2111.3 1 ± 0.94	377.96 ± 0.84	-2.78 ± 0.10	8.077 ± 0.001	8.048 ± 0.001
	Spri ng	19.52 ± 0.04	36.712 ± 0.009	2115.0 5 ± 0.31	2115.3 7 ± 0.51	385.87 ± 0.70	-3.00 ± 0.11	8.073 ± 0.001	8.045 ± 0.001
	Su mm er	22.33 ± 0.06	36.725 ± 0.024	2107.3 6 ± 0.87	2105.7 4 ± 1.26	420.05 ± 0.81	1.99 ± 0.08	8.037 ± 0.001	8.057 ± 0.001
	Aut umn	22.11 ± 0.06	36.754 ± 0.019	2101.8 7 ± 0.63	2098.6 4 ± 1.12	402.98 ± 0.76	0.04 ± 0.13	8.053 ± 0.001	8.069 ± 0.001
	Ann ual	20.99 ± 0.05	36.747 ± 0.016	2108.7 8 ± 0.63	2106.0 6 ± 1.03	397.51 ± 0.77	-0.80 ± 0.11	8.058 ± 0.001	8.057 ± 0.001
CI- SG	Win ter	18.15 ± 0.12	36.595 ± 0.022	2114.1 5 ± 0.96	2120.5 9 ± 1.48	370.31 ± 1.62	-3.10 ± 0.23	8.084 ± 0.002	8.040 ± 0.002
	Spri ng	18.60 ± 0.10	36.418 ± 0.038	2105.9 4 ± 3.43	2122.4 7 ± 1.79	382.90 ± 2.38	-3.01 ± 0.34	8.070 ± 0.002	8.033 ± 0.002
	Su mm er	22.09 ± 0.17	36.580 ± 0.042	2104.0 7 ± 2.88	2112.4 6 ± 1.70	420.70 ± 2.76	1.57 ± 0.24	8.036 ± 0.002	8.052 ± 0.002

Autumn	20.79 ± 0.22	36.650 ± 0.042	2104.4 7 ± 1.53	2107.5 4 ± 2.81	394.50 ± 2.20	-0.43 ± 0.24	8.061 ± 0.002	8.057 ± 0.003
Annual	19.96 ± 0.16	36.582 ± 0.036	2107.4 2 ± 1.97	2115.0 3 ± 2.03	389.99 ± 2.17	-1.34 ± 0.25	8.065 ± 0.002	8.047 ± 0.003

Table 2. Ratios T/B obtained at the selected stations on the GC-TNF, TNF-LNZ and CI-SG routes.

Route	Station	T/B ratios	
GC - TNF	16.05°W	1.94	
	15.7°W	1.60	
	15.6°W	2.10	
TNF - LNZ	15.0°W	2.12	
	14.5°W	1.86	
	13.9°W	1.80	
CI - SG		Open ocean transect	Coastal transect
	29.8°N	1.99	2.03
	30.7°N	1.86	1.65
	31.2°N	1.72	2.09
	33.0°N	2.00	2.25
	34.2°N	2.51	2.46

Table 3. Linear relationships of $f\text{CO}_{2,\text{sw}} - \text{SST}$ and of $f\text{CO}_{2,\text{sw}} - \text{pH}_\text{T}$ in the winter-summer and February-October periods with their respective standard deviations.

Route	Period	$f\text{CO}_2$ (μatm) - SST ($^\circ\text{C}$) relationship	R^2	$f\text{CO}_2$ (μatm) - pH_T (total scale) relationship	R^2
GC - TNF	Winter - Summer	$f\text{CO}_2 = 12.27 (\pm 0.31)$ $\text{SST} + 145.45 (\pm 6.34)$;	0.886	$f\text{CO}_2 = -0.0009 (\pm 1.57 \times 10^{-6})$ $\text{SST} + 8.44 (\pm 6.00 \times 10^{-4})$;	0.999
	February - October	$f\text{CO}_2 = 10.35 (\pm 0.25)$ $\text{SST} + 85.28 (\pm 5.29)$;	0.880	$f\text{CO}_2 = -0.0010 (\pm 2.46 \times 10^{-6})$ $\text{SST} + 8.44 (\pm 1.00 \times 10^{-3})$;	0.999
TNF - LNZ	Winter - Summer	$f\text{CO}_2 = 11.41 (\pm 0.25)$ $\text{SST} + 162.72 (\pm 5.11)$;	0.887	$f\text{CO}_2 = -0.0009 (\pm 1.64 \times 10^{-6})$ $\text{SST} + 8.43 (\pm 6.00 \times 10^{-4})$;	0.999
	February - October	$f\text{CO}_2 = 9.81 (\pm 0.19)$ $\text{SST} + 195.31 (\pm 4.02)$;	0.897	$f\text{CO}_2 = -0.0010 (\pm 1.76 \times 10^{-6})$ $\text{SST} + 8.44 (\pm 7.00 \times 10^{-4})$;	0.999
CI - SG	Winter - Summer	$f\text{CO}_2 = 11.71 (\pm 0.25)$ $\text{SST} + 161.38 (\pm 4.85)$;	0.864	$f\text{CO}_2 = -0.0009 (\pm 3.11 \times 10^{-6})$ $\text{SST} + 8.43 (\pm 1.20 \times 10^{-3})$;	0.996
	February - October	$f\text{CO}_2 = 10.48 (\pm 0.17)$ $\text{SST} + 186.13 (\pm 3.44)$;	0.912	$f\text{CO}_2 = -0.0009 (\pm 2.90 \times 10^{-6})$ $\text{SST} + 8.43 (\pm 1.10 \times 10^{-3})$;	0.997

Table 4. Net contribution on NC_T temporal variation ($\Delta\text{NC}_\text{T}/\text{dt}$) of net community production ($\Delta\text{NC}_\text{T}/\text{dt}|_\text{NCP}$), air-sea exchange ($\Delta\text{NC}_\text{T}/\text{dt}|_\text{EX}$) and horizontal transport ($\Delta\text{NC}_\text{T}/\text{dt}|_\text{TRSP}$) in March-June (spring), June-September (summer) and February-October.

Route	Station	$\Delta\text{NC}_\text{T}/\text{dt}$ (mmol m^{-3})	$\Delta\text{NC}_\text{T}/\text{dt} _\text{EX}$ (mmol m^{-3})	$\Delta\text{NC}_\text{T}/\text{dt} _\text{TRSP}$ (mmol m^{-3})	$\Delta\text{NC}_\text{T}/\text{dt} _\text{NCP}$ (mmol m^{-3})

		Ma rch - Jun e	June - Sept emb er	Febr uary- Octo ber	Ma rch - Jun e	June - Sept emb er	Febr uary- Octo ber	Ma rch - Jun e	June - Sept emb er	Febr uary- Octo ber	Ma rch - Jun e	June - Sept emb er	Febr uary- Octo ber
G C- TN	1	-	-	-	-	-	-	-	-	-	-	-	-
	5. 7°	7.5 2	6.81	10.03	1.0 0	1.30	-0.27	0.2 5	1.28	1.55	6.7 6	6.79	11.31
	1 F- TN	-	-	-	-	-	-	-	-	-	-	-	-
F- LN Z	4. 5°	7.6 7	14.5 5	24.07	1.0 3	1.80	-0.62	0.0 2	0.25	-0.44	6.6 2	12.5 0	23.00
	2	-	-	-	-	-	-	-	-	-	-	-	-
	9. 8°	3.7 5	11.7 1	-8.28	1.3 7	1.44	-0.18	0.0 2	0.03	0.06	2.4 0	10.3 0	-8.16
CI- SG	3 0. 7°	7.5 6	12.7 7	15.01	0.8 0	2.55	-0.88	0.0 1	0.37	-0.49	6.7 5	9.85	13.63
	3 1. 2°	12. 69	16.6 5	27.06	0.2 6	2.67	0.75	0.0 2	0.46	-1.27 x 10 ⁻³	12. 45	13.5 2	26.32
	3 3. 0°	17. 71	6.11	21.59	1.2 1	1.07	-0.22	0.3 0	0.20	0.33	16. 80	4.84	21.70
CI- SG	4. 2°	11. 66	13.8 7	24.17	0.9 0	0.67	-0.09	0.0 5	0.13	-0.19	10. 71	13.0 7	23.88

Figure 1. VOS routes in the region of interest in the Northeast Atlantic. Inter-insular routes between Gran Canaria and Tenerife (GC-TNF) and between Tenerife and Lanzarote (TNF-LNZ) monitor the easternmost part of the Canary basin, while the Canary Islands-Strait of Gibraltar route (CI-SG) monitors the transition zone between coastal and open-ocean waters along northwest Africa. Points marked on the inter-island routes locate the ship's docking ports of Las Palmas de Gran Canaria (GC, red), Santa Cruz de Tenerife (TNF, green) and Arrecife (LNZ, yellow).

Figure 2. Annual and seasonal averages of SST, SSS and CO₂ system parameters and fluxes every 0.05° of longitude on the GC-TNF route (left) and every 0.1° of longitude on the TNF-LNZ routes (right).

Figure 3. Seasonal variability of average (a) SST, (b) SSS and CO₂ system parameters ((c) C_T, (d) NC_T, (e and f) $f\text{CO}_{2,\text{sw}}$, (g) FCO₂ and (h) pH_T and pH_{T,21}) at $16.05 \pm 0.1^\circ\text{W}$ (blue) and $15.7 \pm 0.1^\circ\text{W}$ (red) along the GC-TNF route.

Figure 4. Seasonal variability of average (a) SST, (b) SSS and CO₂ system parameters ((c) C_T, (d) NC_T, (e-h) $f\text{CO}_{2,\text{sw}}$, (i) FCO₂ and (j) pH_T and pH_{T,21}) at $15.6 \pm 0.1^\circ\text{W}$ (blue), $15.0 \pm 0.1^\circ\text{W}$ (red), $14.5 \pm 0.1^\circ\text{W}$ (green) and $13.9 \pm 0.1^\circ\text{W}$ (black) along the TNF-LNZ route.

Figure 5. Annual and seasonal averages of SST, SSS and CO₂ system parameters and fluxes every 0.25° of latitude on the CI-SG route.

Figure 6. Seasonal variability of average SST, $f\text{CO}_{2,\text{sw}}$, FCO₂ and pH_T in open-ocean and coastal waters at points of interest on the CI-SG route located at $29.8 \pm 0.2^\circ\text{N}$, $30.7 \pm 0.2^\circ\text{N}$, and $33.0 \pm 0.2^\circ\text{N}$.

Figure 7. Temporal and longitudinal distribution of the $f\text{CO}_{2,\text{sw}}$ values available in SOCAT (left) and obtained by the CanC A-VOS line (right) in Cape Ghir latitude. Seasonality is given by the harmonic fitting function represented below in red, which is available in Table A.2.

Figure 8. Temporal variation of NC_T ($\Delta\text{NC}_T/\text{dt}$; black) and relative contribution of the terms of net community production ($\Delta\text{NC}_T/\text{dt}|_{\text{NCP}}$; green), air-sea exchange ($\Delta\text{NC}_T/\text{dt}|_{\text{EX}}$; blue) and horizontal transport ($\Delta\text{NC}_T/\text{dt}|_{\text{TRSP}}$; red) from February to October. The net contribution of each term in spring, summer and February-October is shown in Table 4.

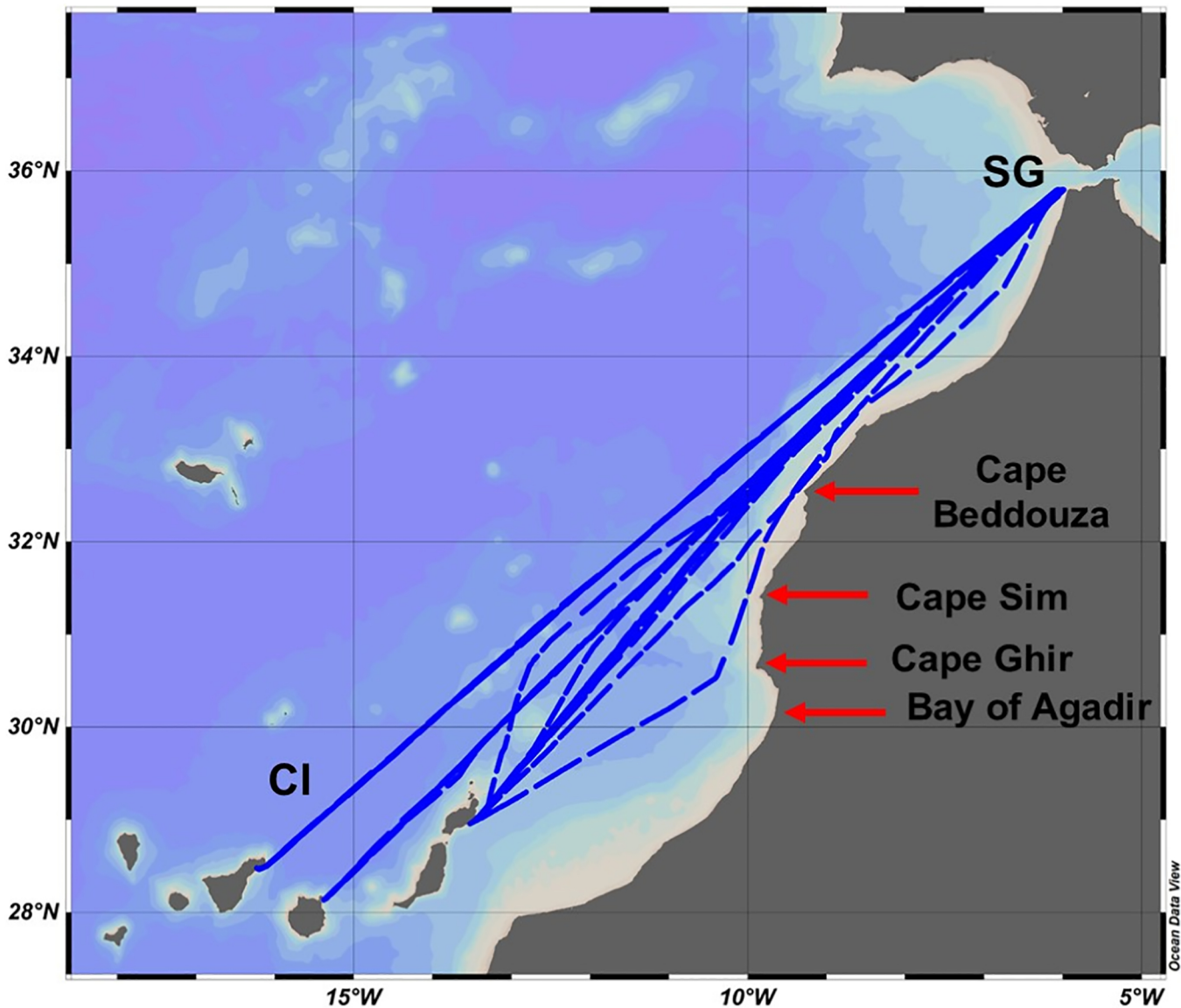
Figure 9. Annual average of FCO₂ (gray), $\Delta f\text{CO}_2$ (red) and wind speed (blue) for each route, calculated with spatial distribution every 0.05° of longitude on the GC-TNF route, 0.1° of longitude on the TNF-LNZ route and 0.25° of latitude on the CI-SG route.

Graphical abstract

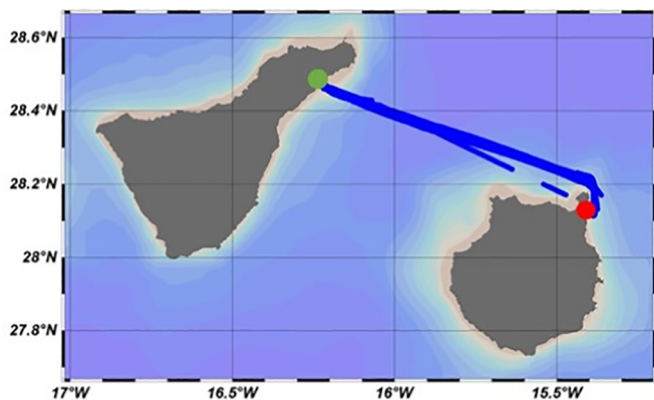
Highlights

- The SST controls the seasonal and spatial variation of CO₂ fugacity and fluxes.
- The pH and *f*CO₂ shows spatial variability associated with upwelling influence.
- NC_T variation was mainly governed by biological activity and slightly affected by air-sea fluxes.
- During 2019, the Northeast Atlantic region behaved as an annual CO₂ sink of -2.65 ± 0.44 Tg CO₂ yr⁻¹.
- VOS lines are a powerful tool to study the CO₂ system and fluxes in the coastal surface area.

Canary Islands – Strait of Gibraltar (CI – SG)



Gran Canaria – Tenerife (GC – TNF)



Tenerife – Lanzarote (TNF – LNZ)

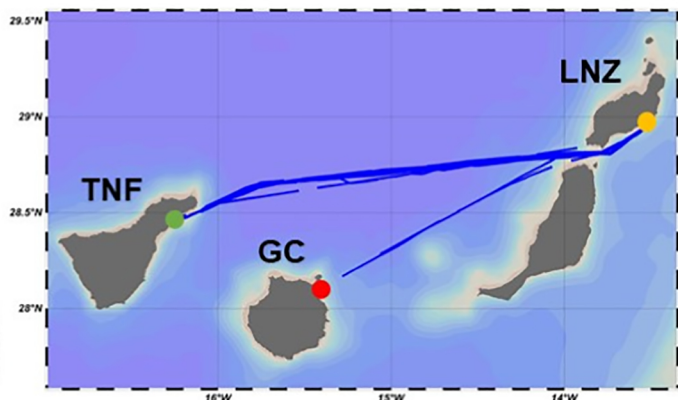


Figure 1

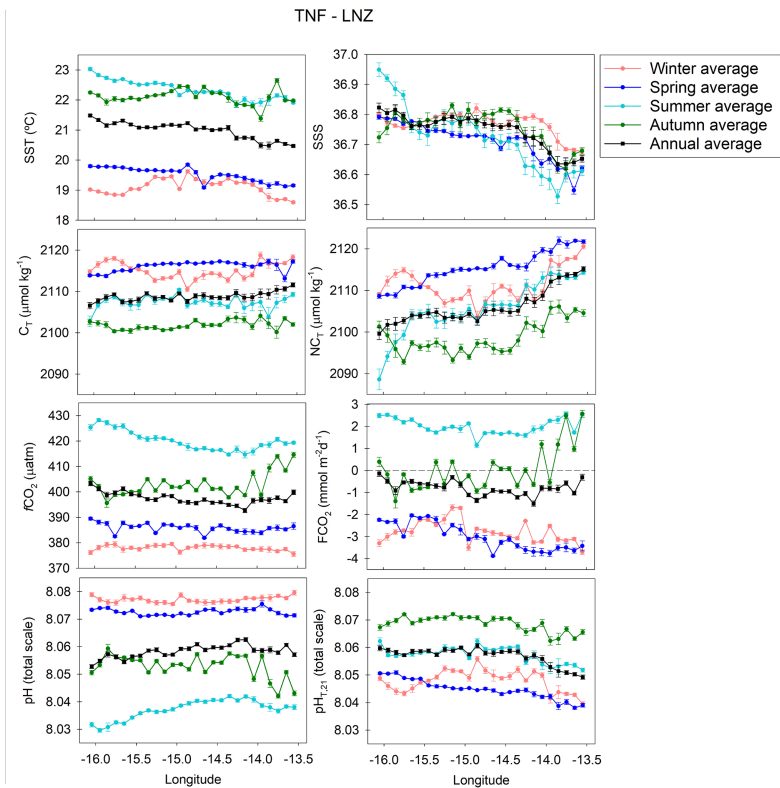
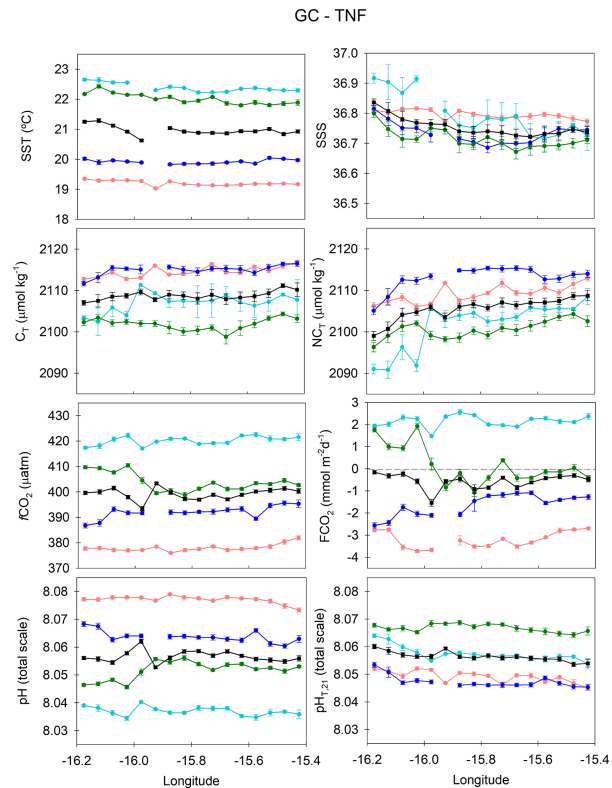


Figure 2

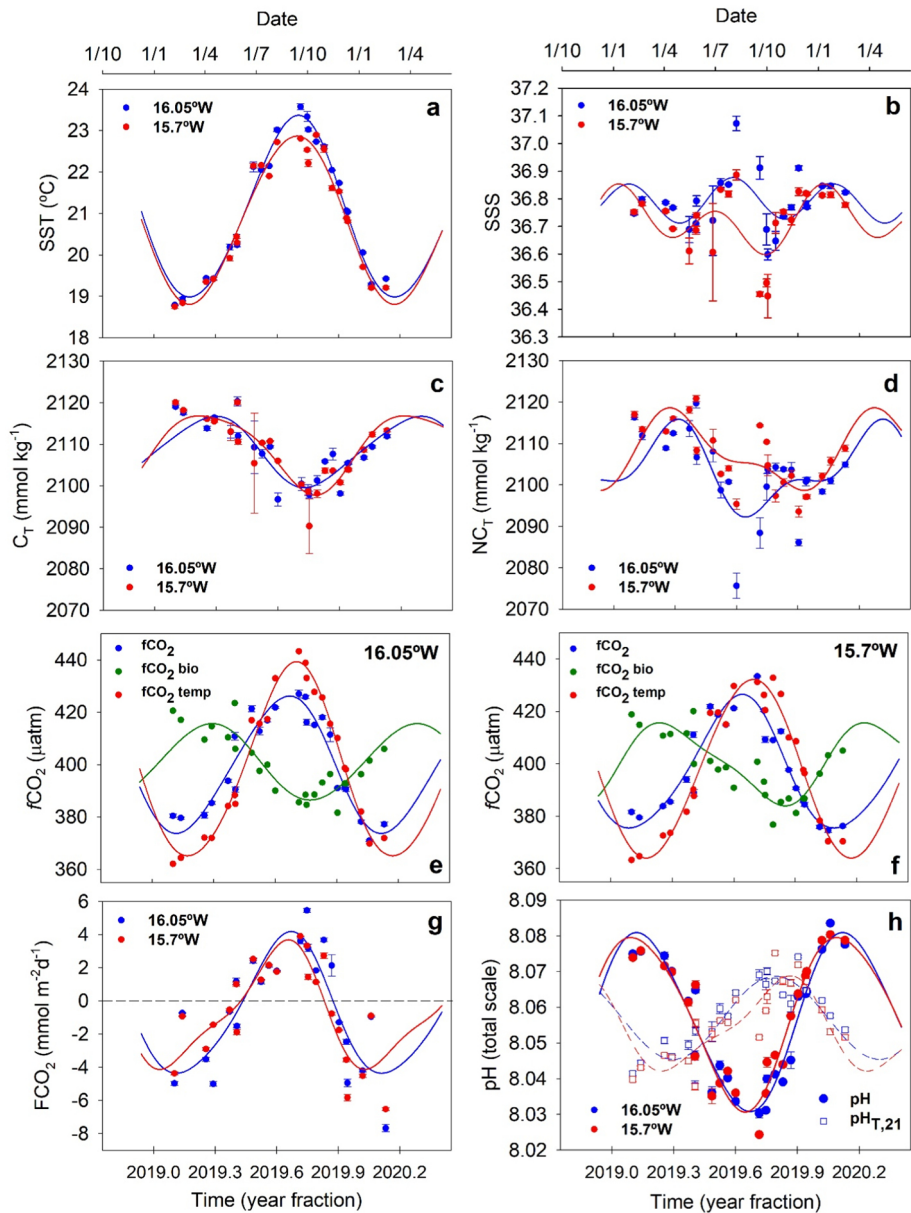


Figure 3

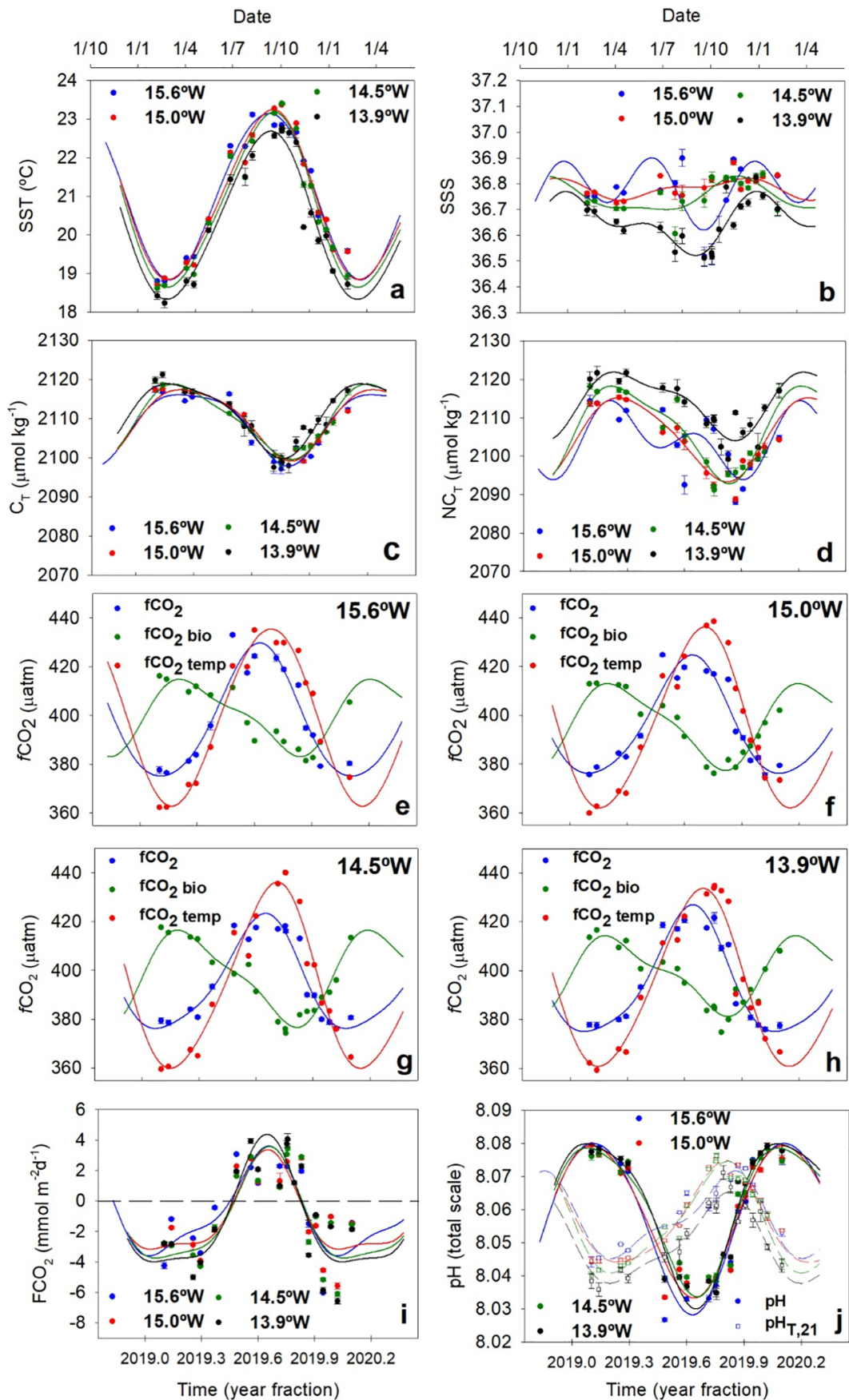


Figure 4

CI - SG

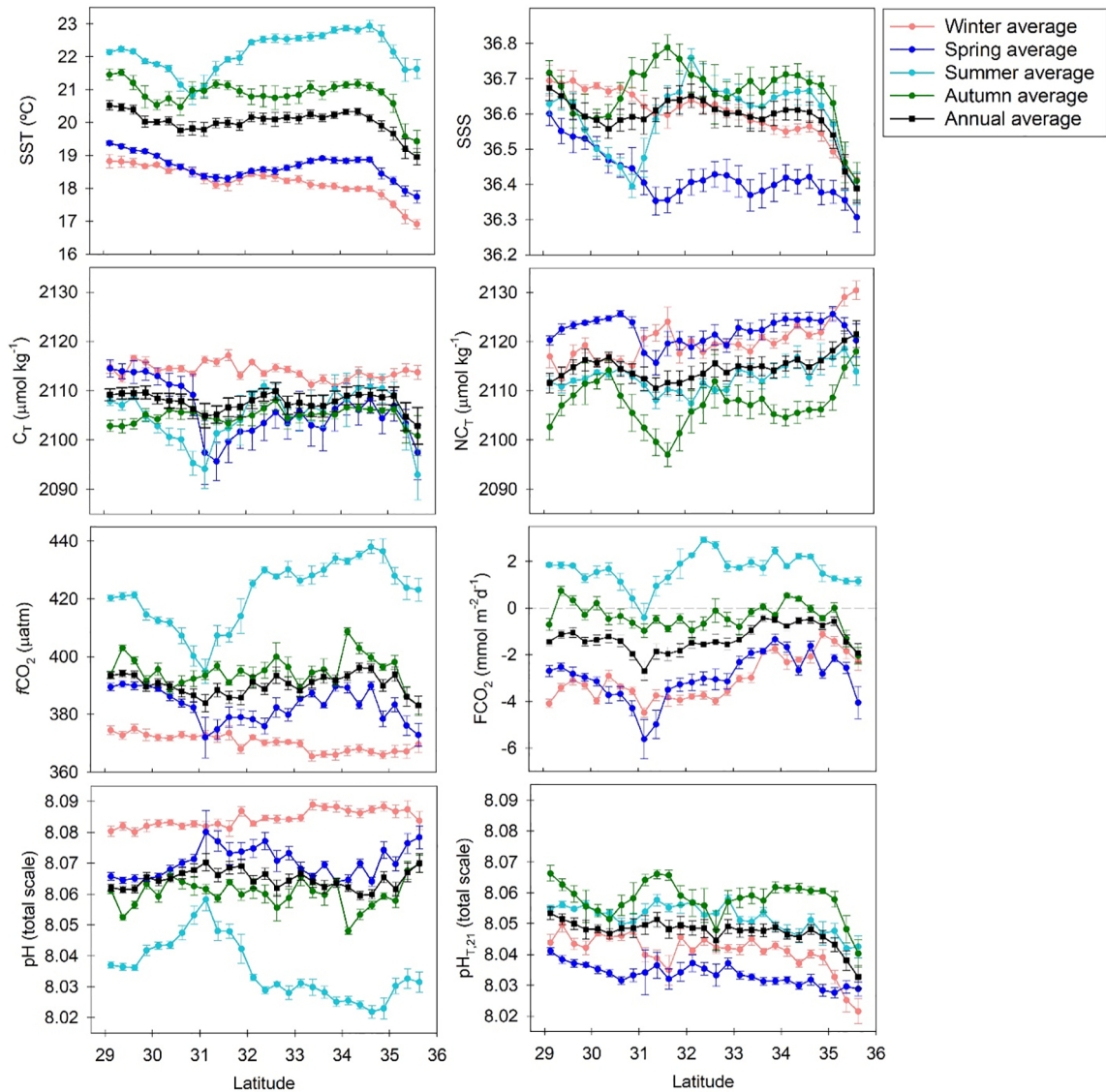


Figure 5

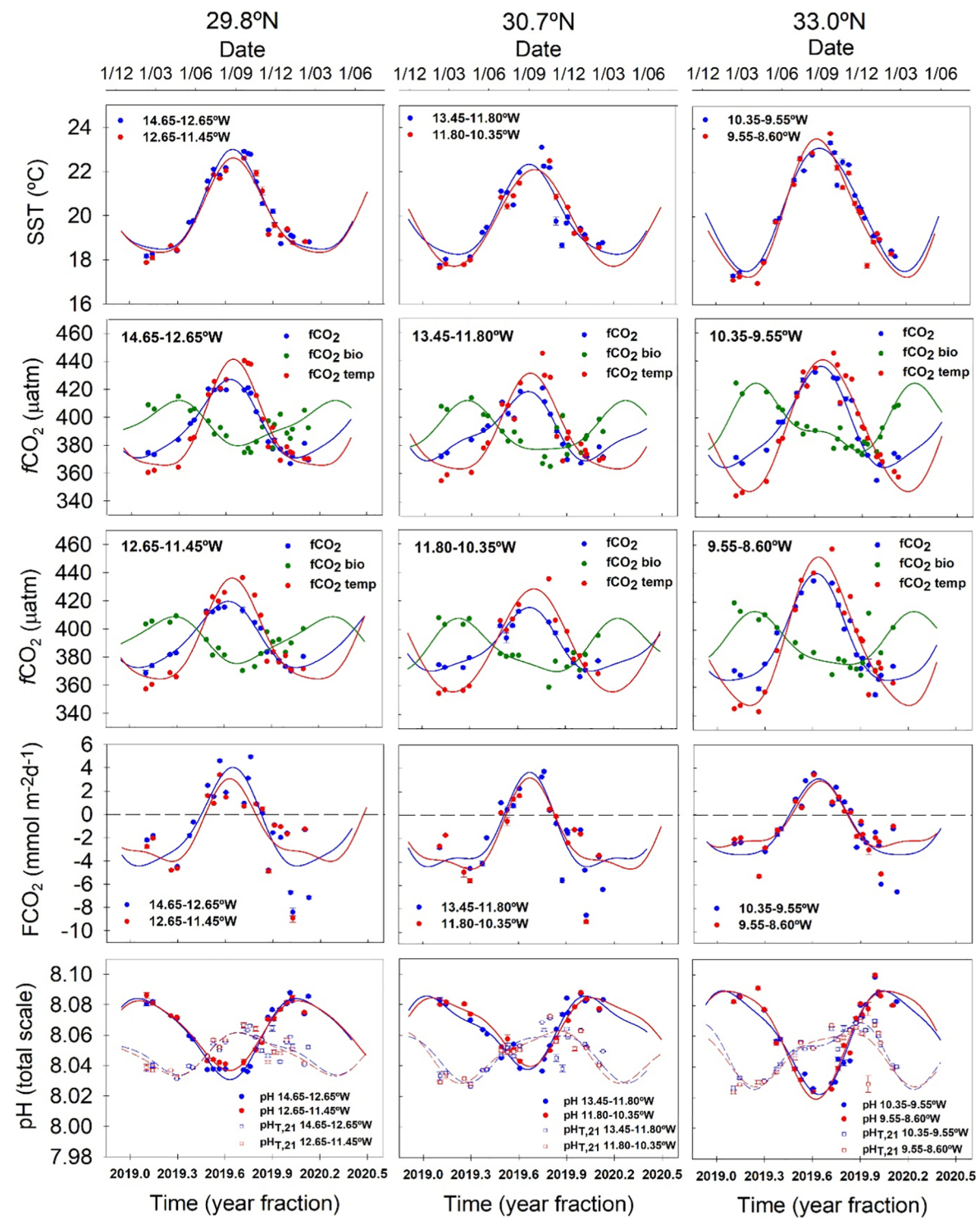


Figure 6

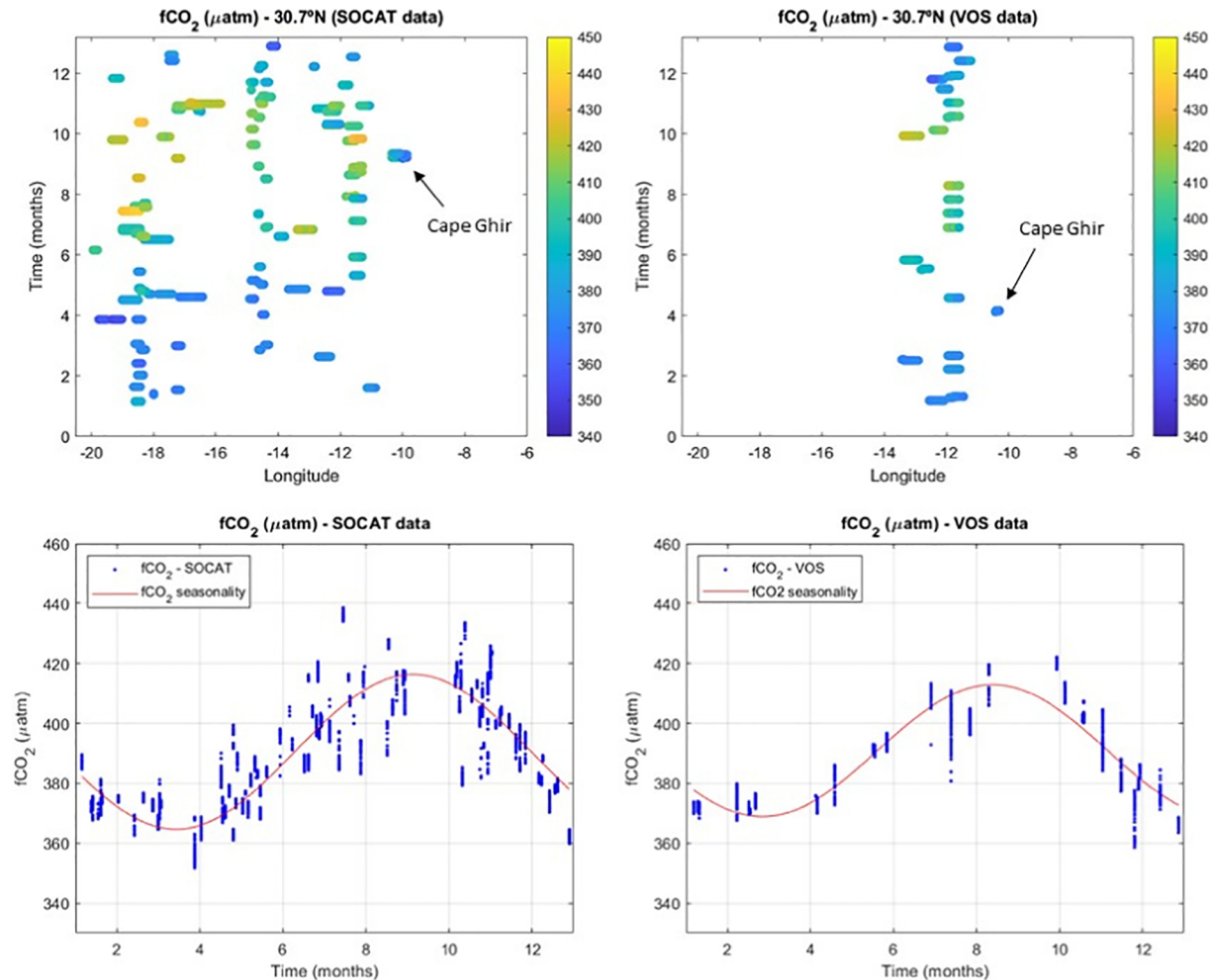


Figure 7

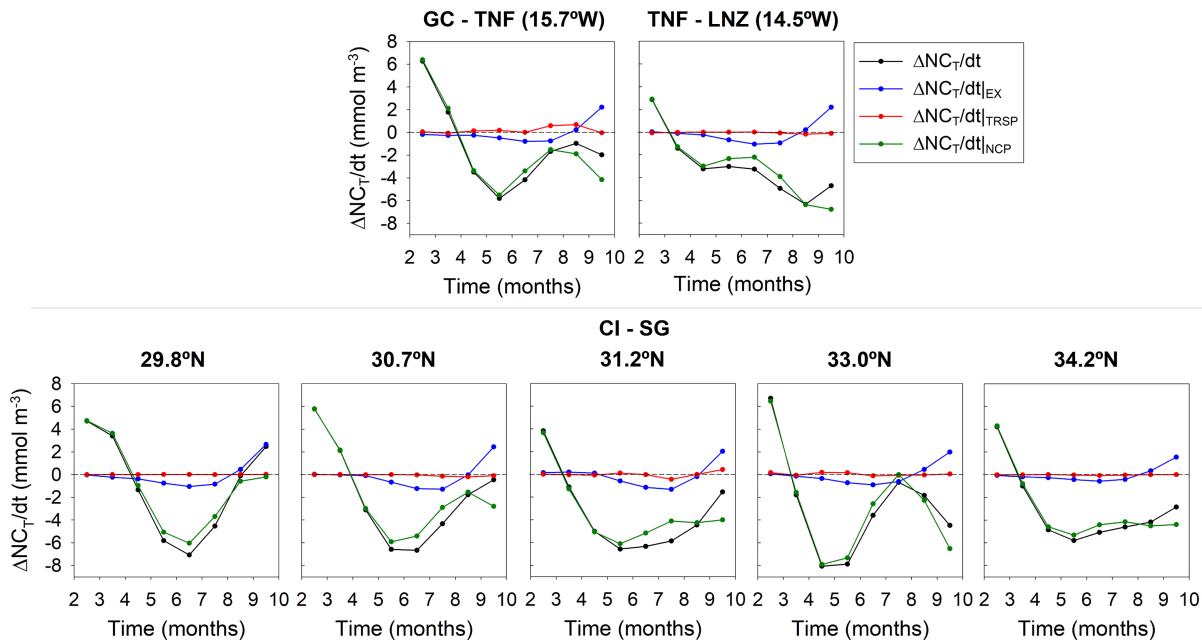


Figure 8

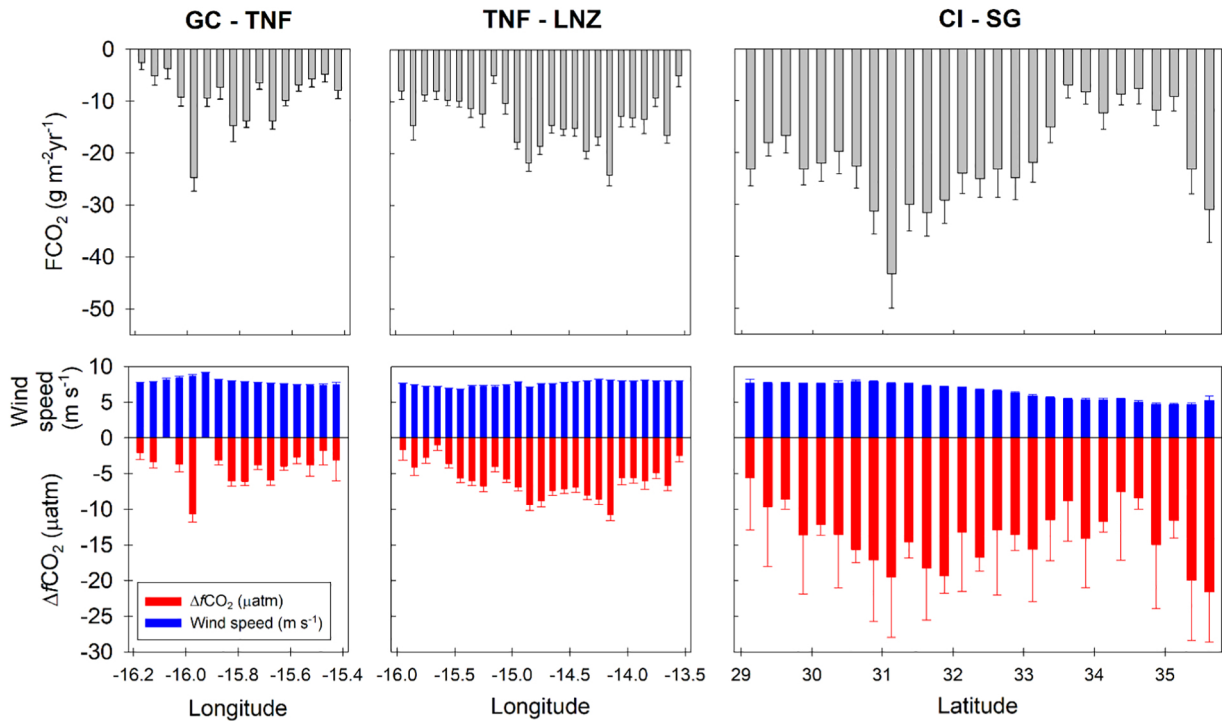


Figure 9